

## Chemical vapor deposition of trimethylaluminium on dealuminated faujasite zeolite

**Citation for published version (APA):**

Pidko, E. A., Almutairi, S. M. T., Mezari, B., Magusin, P. C. M. M., & Hensen, E. J. M. (2013). Chemical vapor deposition of trimethylaluminium on dealuminated faujasite zeolite. *ACS Catalysis*, 3(7), 1504-1517. <https://doi.org/10.1021/cs400181p>

**DOI:**

[10.1021/cs400181p](https://doi.org/10.1021/cs400181p)

**Document status and date:**

Published: 01/01/2013

**Document Version:**

Accepted manuscript including changes made at the peer-review stage

**Please check the document version of this publication:**

- A submitted manuscript is the version of the article upon submission and before peer-review. There can be important differences between the submitted version and the official published version of record. People interested in the research are advised to contact the author for the final version of the publication, or visit the DOI to the publisher's website.
- The final author version and the galley proof are versions of the publication after peer review.
- The final published version features the final layout of the paper including the volume, issue and page numbers.

[Link to publication](#)

**General rights**

Copyright and moral rights for the publications made accessible in the public portal are retained by the authors and/or other copyright owners and it is a condition of accessing publications that users recognise and abide by the legal requirements associated with these rights.

- Users may download and print one copy of any publication from the public portal for the purpose of private study or research.
- You may not further distribute the material or use it for any profit-making activity or commercial gain
- You may freely distribute the URL identifying the publication in the public portal.

If the publication is distributed under the terms of Article 25fa of the Dutch Copyright Act, indicated by the "Taverne" license above, please follow below link for the End User Agreement:

[www.tue.nl/taverne](http://www.tue.nl/taverne)

**Take down policy**

If you believe that this document breaches copyright please contact us at:

[openaccess@tue.nl](mailto:openaccess@tue.nl)

providing details and we will investigate your claim.

## Chemical vapor deposition of trimethylaluminium on dealuminated faujasite zeolite

Evgeny A Pidko, Sami Almutairi, Brahim Mezari, Pieter C.M.M. Magusin, and Emiel J. M. Hensen

ACS Catal., Just Accepted Manuscript • DOI: 10.1021/cs400181p • Publication Date (Web): 31 May 2013

Downloaded from <http://pubs.acs.org> on June 4, 2013

### Just Accepted

“Just Accepted” manuscripts have been peer-reviewed and accepted for publication. They are posted online prior to technical editing, formatting for publication and author proofing. The American Chemical Society provides “Just Accepted” as a free service to the research community to expedite the dissemination of scientific material as soon as possible after acceptance. “Just Accepted” manuscripts appear in full in PDF format accompanied by an HTML abstract. “Just Accepted” manuscripts have been fully peer reviewed, but should not be considered the official version of record. They are accessible to all readers and citable by the Digital Object Identifier (DOI®). “Just Accepted” is an optional service offered to authors. Therefore, the “Just Accepted” Web site may not include all articles that will be published in the journal. After a manuscript is technically edited and formatted, it will be removed from the “Just Accepted” Web site and published as an ASAP article. Note that technical editing may introduce minor changes to the manuscript text and/or graphics which could affect content, and all legal disclaimers and ethical guidelines that apply to the journal pertain. ACS cannot be held responsible for errors or consequences arising from the use of information contained in these “Just Accepted” manuscripts.

1  
2  
3  
4  
5  
6  
7  
8  
9  
10  
11  
12  
13  
14  
15  
16  
17  
18  
19  
20  
21  
22  
23  
24  
25  
26  
27  
28  
29  
30  
31  
32  
33  
34  
35  
36  
37  
38  
39  
40  
41  
42  
43  
44  
45  
46  
47  
48  
49  
50  
51  
52  
53  
54  
55  
56  
57  
58  
59  
60

# Chemical vapor deposition of trimethylaluminum on dealuminated faujasite zeolite

*Evgeny A. Pidko\**, *Sami M.T. Almutairi*, *Brahim Mezari*, *Pieter C.M.M. Magusin*,

*Emiel J.M. Hensen\**

Schuit Institute of Catalysis, Laboratory of Inorganic Materials Chemistry, Eindhoven University  
of Technology, Den Dolech 2, 5600 MB Eindhoven, The Netherlands

KEYWORDS: faujasite, dealumination, chemical vapor deposition, trimethylaluminum,  
extraframework aluminum, propane cracking, H/D exchange, NMR, acidity, infrared  
spectroscopy

## ABSTRACT

Chemical vapor deposition of trimethylaluminum (TMA) was explored as an approach for the preparation of model faujasite-type catalysts containing extraframework aluminum. The decomposition of the grafted organoaluminum species was investigated in hydrogen and oxygen atmosphere. The process of grafting Al-containing species and the associated changes of the zeolite hydroxyl groups were followed by in situ FTIR spectroscopy. The state of intrazeolite Al atoms, the changes in zeolite structure and acidity caused by the CVD procedure as well as by subsequent treatment were analyzed in detail by  $^1\text{H}$ ,  $^{29}\text{Si}$  and  $^{27}\text{Al}$  MAS NMR,  $\text{CO}_{\text{ads}}$  IR, H/D exchange of acidic hydroxyl groups with perdeuterobenzene and propane cracking. Reaction of an extraframework aluminum-free high-silica faujasite zeolite with TMA leads to nearly complete substitution of the bridging hydroxyl groups with Al species. The reaction, however, does not produce uniform homogeneously distributed species. Because of the high reactivity of TMA, the zeolite lattice is partially decomposed resulting in its partial dealumination and formation of stable Si-CH<sub>3</sub> moieties. The exact conditions of post-CVD treatment influence strongly the chemical and catalytic properties of the zeolites. The strongest increase of the propane conversion rate was observed when grafted TMA species were decomposed in H<sub>2</sub> at high temperature. Such zeolite displays much higher activity per Brønsted acid site in propane cracking than a commercial ultrastabilized Y zeolite. It is proposed that the activity enhancement is related to strong polarization of a fraction of the zeolite Brønsted acid sites by Lewis acid sites formed by the hydrogenolysis of grafted TMA complexes.

## 1. Introduction

Zeolites are extensively used in the oil refining and petrochemical industry as acid catalysts to crack carbon-carbon bonds, isomerize and oligomerize alkenes and alkylate aromatics.<sup>1-2</sup> Zeolite acidity is understood to a significant degree.<sup>3-5</sup> Acid catalytic activity resides at sites involving tetrahedral aluminum species substituting silicon atoms in the framework. Zeolite Y, the preferred zeolite in hydrocracking catalysts, has the faujasite structure which features a single crystallographic tetrahedral site. Ideally, at high Si/Al ratios dilute Brønsted acid sites (BAS) in a pure faujasite material will therefore be equivalent.<sup>6</sup> After hydrothermal synthesis of zeolite Y, its Al content is high (Si/Al = 2.5), while its stability and acidity are low. The low acidity is understood in terms of the next-nearest neighbor model.<sup>7</sup> According to this model, bridging hydroxyl groups in Al-rich regions of zeolites have the strongest O-H bonds because of higher basicity of lattice oxygens. In practice, a hydrocracking catalyst will contain steam-calcined stabilized faujasites with Si/Al molar ratios in the 4.5-50 range. The steam calcination procedure renders the zeolite more stable and acidic and also creates additional mesoporosity. Even in simple test reactions, like cracking or hydroconversion of alkanes, materials of similar composition show hugely different activities. The usual interpretation of such differences involves the assumption that zeolitic acid sites can differ in strength. Non-framework aluminum species due to partial framework dealumination can boost the activity of zeolites in cracking reactions or affect its selectivity.<sup>8,9</sup> These strongly Lewis acidic aluminum species do not seem to contribute to protolytic cracking, but instead are believed to enhance the strength of Brønsted acid sites in their vicinity<sup>10,11</sup> and to promote alternative alkane activation paths such as dehydrogenation.<sup>12</sup>

1  
2  
3 The extracted Al atoms form the commonly named extraframework Al (EFAl) phase, which  
4 includes charged complexes at cationic positions and neutral aggregates occluded in the  
5 micropore space.<sup>13-15</sup> Part of the EFAl phase may also be located in the mesopores or at the  
6 external surface. Due to the heterogeneous nature of the EFAl phase, it has not been possible yet  
7 to unambiguously determine the structure of such species nor their role in catalytic cracking  
8 reactions. The formation of EFAl species in the zeolite pores is believed to increase acidity. The  
9 nature of these EFAl species and how they affect Brønsted acidity of zeolites is an issue of  
10 continuous debate. It has been postulated that these EFAl polarize neighboring BAS and increase  
11 their activity in acid-catalyzed reactions.<sup>16</sup> In recent work, Iglesia and co-workers opposed this  
12 view by suggesting that the activity enhancement is mainly associated with the change of  
13 effective void of the supercage due to the presence of EFAl rather than to changes in intrinsic  
14 strength of BAS.<sup>17</sup> On contrary, van Bokhoven and co-workers demonstrated that EFAl species  
15 in steam-activated zeolite Y predominantly occupy cationic positions in the sodalite cages and,  
16 therefore, cannot directly influence the adsorption of hydrocarbons in the supercages.<sup>18</sup>  
17  
18  
19  
20  
21  
22  
23  
24  
25  
26  
27  
28  
29  
30  
31  
32  
33  
34  
35  
36

37 The introduction of extraframework Al in low-silica X and Y zeolite results in a substantial  
38 increase of acidity of BAS.<sup>19</sup> Solid-state NMR spectroscopy is a powerful method for the  
39 investigation of the oxygen coordination, local symmetry and concentration of Al atoms at  
40 framework and extraframework positions in zeolites. Many efforts have focussed on  
41 understanding the role of EFAl on BAS using different NMR spectroscopic techniques such as  
42 <sup>1</sup>H DQ-MAS NMR and <sup>13</sup>C MAS NMR of adsorbed 2-<sup>13</sup>C-acetone.<sup>20-22</sup> It was also used to  
43 reveal the importance of the spatial proximity of Brønsted and Lewis acid sites in dealuminated  
44 H-Y zeolite to enhance acidity.<sup>23-25</sup> More recently,<sup>26</sup> also <sup>27</sup>Al DQ-MAS NMR spectroscopy was  
45 employed to study the location of various types of Al species in dealuminated Y zeolite. Besides,  
46  
47  
48  
49  
50  
51  
52  
53  
54  
55  
56  
57  
58  
59  
60

1  
2  
3 several studies employed monomolecular cracking of hydrocarbons to characterize the intrinsic  
4 reactivity of the zeolitic Brønsted acid sites of different zeolites.<sup>27-34</sup> One of the reasons why it  
5  
6 remains difficult to draw clear conclusions on the structure and role of EFAl is the significant  
7  
8 structural heterogeneity of EFAl-containing faujasites.  
9  
10

11  
12  
13  
14 In order to understand better the nature and catalytic role of EFAl in faujasite zeolites, it  
15  
16 would be useful to develop model zeolites containing well-defined EFAl species. In our previous  
17  
18 work, the influence of extraframework Al in a model high-silica faujasite (Si/Al  $\approx$  5, no EFAl)  
19  
20 introduced by conventional methods such as incipient wetness impregnation and ion exchange  
21  
22 was investigated.<sup>35</sup> Strong synergy in propane conversion was observed between BAS and  
23  
24 cationic EFAl species. Despite efforts to control the type of Al species, it was found that there  
25  
26 remains a considerable degree of heterogeneity in such model samples.  
27  
28  
29  
30

31  
32 The surface organometallic approach involves modification of solid surfaces by catalytically  
33  
34 active species by selective reaction of its functional groups.<sup>36</sup> In zeolites the hydroxyl groups will  
35  
36 react with volatile metal-alkyl species. This approach has been explored before for preparation of  
37  
38 model systems of Ga/ZSM-5.<sup>37,38</sup> It has also been used to modify ZSM-5 with Zn cations.<sup>39</sup> The  
39  
40 reaction of Brønsted acid sites and the highly reactive organometallic precursor results in well-  
41  
42 defined cationic surface species, which can be further modified by subsequent thermochemical  
43  
44 activation. Herein, the use of volatile trimethylaluminum (Al(CH<sub>3</sub>)<sub>3</sub>, TMA) is explored as a  
45  
46 potential precursor for well-defined EFAl species in zeolite Y. Previously, it has been  
47  
48 demonstrated that TMA can be effectively incorporated into mesoporous silica MCM-41 via  
49  
50 various post-synthesis procedures.<sup>40</sup> TMA itself is a prototypical precursor to the industrially  
51  
52 important MAO co-catalyst for olefin polymerization.<sup>41-55</sup> The modification of dealuminated Y  
53  
54  
55  
56  
57  
58  
59  
60

1  
2  
3 zeolite with TMA followed by impregnation of platinum has been shown to result in enhanced  
4 reactivity of the zeolite catalyst for decane dehydrogenation.<sup>56-58</sup>  
5  
6  
7

8  
9 As a starting material, we employ a high-silica faujasite zeolite prepared by selective  
10 substitution of Al<sub>F</sub> with Si atoms via treatment with ammonium hexafluorosilicate (NH<sub>4</sub>)<sub>2</sub>SiF<sub>6</sub> of  
11 zeolite Y.<sup>7,35</sup> EFAl species were then introduced by chemical vapor deposition of TMA followed  
12 by the decomposition of the grafted organoaluminum species under oxidizing or reducing  
13 conditions. The state of EFAl in the prepared materials was investigated by <sup>27</sup>Al MAS NMR  
14 spectroscopy and FTIR spectroscopy of adsorbed CO. Brønsted acidity of the zeolite catalysts  
15 was investigated by monitoring the selective H/D exchange of acidic hydroxyl groups with C<sub>6</sub>D<sub>6</sub>  
16 by IR spectroscopy.<sup>59-62</sup> The acid catalytic activity of these zeolites was determined by propane  
17 cracking experiments.  
18  
19  
20  
21  
22  
23  
24  
25  
26  
27  
28  
29

## 30 31 **2. Experimental**

### 32 33 *2.1. Catalyst preparation*

34  
35  
36 Dealuminated AHFSY zeolite was prepared according to the procedure described in Ref. 35  
37 (AHFSY-60) by reacting the ammonium form of zeolite Y (Akzo Nobel, Si/Al = 2.5) zeolite  
38 with an aqueous solution of ammonium hexafluorosilicate ((NH<sub>4</sub>)<sub>2</sub>SiF<sub>6</sub>, AHFS). The framework  
39 Si/Al ratio in the resulting AHFSY material was 4.2. Subsequent modification with  
40 trimethylaluminum was performed by chemical vapor deposition (CVD) of Al(CH<sub>3</sub>)<sub>3</sub>  
41 (trimethylaluminum, TMA, Alderich Chemicals, 95%) on dehydrated AHFSY zeolite. Prior to  
42 the TMA CVD treatment, the AHFSY powder was pressed, crushed and sieved to a fraction  
43 between 250 and 500 μm. The catalyst was calcined in a mixture of 20 vol. % oxygen in nitrogen  
44 at a flow rate of 100 Nml/min whilst heating at a heating rate of 2 °C/min followed by an  
45  
46  
47  
48  
49  
50  
51  
52  
53  
54  
55  
56  
57  
58  
59  
60



1  
2  
3 isothermal period of 6 h to obtain the hydrogen form of AHFSY. The dehydrated catalyst was  
4 transferred into a nitrogen-flushed glove-box without exposure to air. All subsequent  
5 manipulations were performed under inert atmosphere. To a glass vessel containing a small  
6 sample bottle with 1 g of dehydrated AHFSY, 1 ml of TMA was added (see supporting  
7 information). After CVD for 48 h, the material was evacuated for 2 h to remove unreacted  
8 trimethylaluminum and reaction products. The modified zeolite was then kept under inert  
9 atmosphere. Before the catalytic tests, the TMA-modified samples were either treated in pure H<sub>2</sub>  
10 for 2 h at 550 °C and/or calcined in a mixture of 20% O<sub>2</sub> in He. The activated catalysts were  
11 denoted as AHFSY-TMA-Red, AHFSY-TMA-Red-Oxd and AHFSY-TMA-Oxd, respectively,  
12 for the catalyst activated by reduction in H<sub>2</sub>, a cycle of reduction-oxidation and oxidation in O<sub>2</sub> at  
13 550 °C.  
14  
15  
16  
17  
18  
19  
20  
21  
22  
23  
24  
25  
26  
27  
28  
29

## 30 2.2. Catalyst characterization

### 31 *X-Ray diffraction (XRD)*

32  
33 XRD patterns of zeolites were recorded on a Bruker D4 Endeavor Diffractometer using Cu K $\alpha$   
34 radiation with a wavelength of 1.54056 Å. 2 $\theta$  angles from 5° to 60° were measured with a step  
35 size of 0.077° and a time per step of 1 s. The catalysts were ground and pressed in sample  
36 holders for measurements under ambient conditions. Crystallinity of the zeolite samples was  
37 calculated from the XRD patterns using the Topas software.  
38  
39  
40  
41  
42  
43  
44  
45  
46

### 47 *Elemental analysis*

48  
49 The aluminum content in zeolite catalysts was determined by elemental analysis, which was  
50 carried out by ICP-OES (Spectro Ciros CCD ICP optical emission spectrometer with axial  
51 plasma viewing). For the ICP measurements the samples were dissolved in a 1.5 mL solution of  
52 HF/HNO<sub>3</sub>/H<sub>2</sub>O (1:1:1) acid mixture.  
53  
54  
55  
56  
57  
58  
59  
60

### *Argon porosimetry*

Surface area and porosity of the zeolites were determined by argon physisorption. In a typical experiment, a dehydrated zeolite sample (~100 mg) was loaded in the sample holder inside a N<sub>2</sub>-flushed glove-box and outgassed at room temperature prior to the sorption measurement. The measurements were performed in static mode at -186 °C on a Micromeritics ASAP-2020 apparatus. The Brunauer-Emmett-Teller (BET) equation was used to calculate the specific surface area from the adsorption data obtained in the p/p<sub>0</sub> range of 0.05-0.25. The volume of mesopores was calculated using the Barrett-Joyner-Halenda (BJH) method on the adsorption branch of the isotherm.

### *Fourier transform infrared spectroscopy (FTIR)*

FTIR spectra were recorded with a Bruker Vertex V70 FTIR spectrometer in transmission mode. Typically, about 10 mg zeolite sample was pressed into a self-supporting wafer (density of 5.0-6.0 mg/cm<sup>2</sup>) and placed in a controlled-environment transmission cell. The spectra were normalized to the thickness of the wafer, determined from the weights of the sample in the dehydrated state. Prior to recording spectra, the zeolites were dehydrated in an O<sub>2</sub> flow whilst heating from room temperature to 550 °C at a heating rate of 5 °C/min. After an isothermal period of 1 h at 550 °C, the sample was evacuated for 50 min at 550 °C and cooled to room temperature in vacuum.

The reaction of TMA with zeolite Brønsted acid sites and the subsequent conversion of the grafted species was monitored in situ by FTIR spectroscopy. The zeolite AHFSY wafer was loaded in the cell, dehydrated and evacuated followed by a short exposure to TMA vapor at room temperature. After a hold time of 20 min, the sample was evacuated for 2 h and subsequently either reduced (H<sub>2</sub>) or oxidized (O<sub>2</sub>) at a pressure of 50 mbar and increasing temperatures (100,

1  
2  
3 200, 300, 400 and 500 °C) for 30 min followed by evacuation at each temperature setting and  
4  
5 recording an FTIR spectrum.  
6  
7

#### 8 9 *Acidity characterization by H/D exchange with perdeuterated benzene*

10  
11 The intrinsic acidity of different faujasite zeolites was probed using a methodology based on  
12 the selective H/D exchange of hydroxyl groups in the zeolite upon the reaction with  
13 perdeuterated benzene.<sup>59-62</sup> The progress of the H/D exchange reaction was monitored in situ by  
14 infrared spectroscopy. FTIR spectra were recorded with a Bruker Vertex V70v FTIR  
15 spectrometer in transmission mode following the procedure described in Ref. 35.  
16 Perdeuterobenzene (C<sub>6</sub>D<sub>6</sub>, Aldrich, purity 99.96%) was dosed into the cell containing a  
17 dehydrated zeolite sample from a glass ampoule via a computer controlled pneumatic valve. The  
18 total volume of C<sub>6</sub>D<sub>6</sub> administered to the cell was 0.33 mmol. The sample was exposed to C<sub>6</sub>D<sub>6</sub>  
19 for 10 s followed by evacuation for 1 h. Then a next spectrum of the partially exchanged sample  
20 was recorded. This sequence was automatically repeated to collect spectra for partially  
21 exchanged samples with exposure times of 30 s, 5 min, 10 min, 20 min, and 30 min at 30 °C, 30  
22 min and 60 min at 50 °C, 30 min at 100 °C. Difference spectra were obtained by subtracting the  
23 initial spectrum of the dehydrated sample from the spectra after exposure to C<sub>6</sub>D<sub>6</sub>.  
24  
25  
26  
27  
28  
29  
30  
31  
32  
33  
34  
35  
36  
37  
38  
39  
40  
41

#### 42 *Infrared spectroscopy of adsorbed CO*

43  
44 Infrared spectroscopy measurements of adsorbed CO were performed at a liquid nitrogen  
45 temperature using a controlled atmosphere transmission cell equipped cooled by flowing liquid  
46 nitrogen through a capillary spiraled around the catalyst wafer. After the liquid temperature was  
47 reached an initial spectrum was recorded. CO was dosed via a sample loop connected to a six-  
48 way valve (50 µl). FTIR spectra were recorded by accumulating 64 scans at a resolution of 2  
49  
50  
51  
52  
53  
54  
55  
56  
57  
58  
59  
60

1  
2  
3 cm<sup>-1</sup>. Difference spectra were obtained by subtracting the initial spectrum of the dehydrated  
4  
5 catalyst from the spectra obtained at increasing CO coverage.  
6  
7

8 More detailed descriptions of the characterization procedures can be found in Refs. 34,39.  
9

### 10 *Solid-state NMR*

11  
12 NMR experiments were performed in a magnetic field of 11.7 Tesla on a Bruker Avance  
13 DMX500 operating at 500 MHz for <sup>1</sup>H, 99 MHz for <sup>29</sup>Si and 132 MHz for <sup>27</sup>Al. The NMR  
14  
15 measurements were carried out using a 4-mm MAS probehead with a sample rotation rates of  
16  
17 12.5 kHz for <sup>1</sup>H and <sup>27</sup>Al, and 10 KHz for <sup>29</sup>Si NMR measurements.  
18  
19  
20  
21

22  
23 <sup>1</sup>H NMR spectra were recorded with a Hahn-echo pulse sequence p1-τ1-p2-τ2-aq with a 90°  
24 pulse p1=5 μs and a 180° p2=10 μs. The interscan delay of 120 s was chosen for quantitative  
25 spectra. Quantitative <sup>29</sup>Si NMR spectra were recorded using a High Power proton Decoupling  
26 direct excitation (DE) pulse sequence with a 90° pulse duration of 5 μs and an interscan delay of  
27 360 s. <sup>1</sup>H-<sup>29</sup>Si cross-polarization (CP) spectra were obtained using an interscan delay of 3 s and a  
28 contact time of 5 ms. <sup>27</sup>Al NMR spectra were recorded with a single pulse sequence with a 18°  
29 pulse duration of 1 μs and a interscan delay of 1 s. MQMAS spectra were recorded by use of the  
30 three-pulse sequence p1-t1-p2-τ-p3-t2 for triple-quantum generation and zero-quantum filtering  
31 (strong pulses p1 = 3.4 μs and p2 = 1.4 μs at ν1= 100 kHz; soft pulse p3 = 11 μs at ν1= 8 kHz;  
32 filter time τ =20 μs; interscan delay 0.2 s). <sup>1</sup>H-<sup>27</sup>Al} TRAnsfer of Population in DOuble  
33 Resonance (TRAPDOR) spectra were recorded by use of a 90°-τ1-180°-τ2 proton pulse sequence  
34 with equal time intervals τ1= τ2 = 795 μs and with irradiation at the <sup>27</sup>Al NMR frequency, during  
35 τ1. The same experiment without <sup>27</sup>Al irradiation served as a blank experiment for reference. The  
36 interscan delay was 10 s. Tetramethylsilane (TMS) was used for calibrating the <sup>1</sup>H and <sup>29</sup>Si NMR  
37 shift, and a concentrated Al(NO<sub>3</sub>)<sub>3</sub> solution for <sup>27</sup>Al NMR shift calibration.  
38  
39  
40  
41  
42  
43  
44  
45  
46  
47  
48  
49  
50  
51  
52  
53  
54  
55  
56  
57  
58  
59  
60

1  
2  
3 The different TMA modified AHFSY zeolites were loaded in a 4-mm zirconia NMR rotor in a  
4 nitrogen-flushed glove box and tightly closed with a Kel-F cap. After that, the rotor was  
5 transferred to the NMR probe under nitrogen gas atmosphere.  
6  
7  
8  
9

### 10 11 12 13 *2.3. Catalytic activity measurements*

14  
15 Similar to our previous study,<sup>35</sup> the acid activity of the zeolites was determined by measuring  
16 the rate of monomolecular cracking of propane. Catalytic activity measurements were performed  
17 in an atmospheric-pressure single-pass quartz microflow reactor at 590 °C. The reactor was  
18 loaded with the catalyst under inert atmosphere. The feed mixture was delivered by thermal mass  
19 flow controllers and consisted of 10 vol. % C<sub>3</sub>H<sub>8</sub> in He (Linde gas) at a total flow rate of 100  
20 ml/min. The WHSV space velocity was kept at 11.7 h<sup>-1</sup>. The product composition was analyzed  
21 by an online three-column gas chromatograph (Compact GC Interscience) equipped with a  
22 PLOT Al<sub>2</sub>O<sub>3</sub>/KCl column with a flame ionization detector and Molsieve-5 Å and RTX-1  
23 columns both employing thermal conductivity detectors. The conversion was kept below 2% to  
24 ensure differential conditions. The reaction rates ( $r$ ) were calculated according to  $r =$   
25  $X \cdot F / m_{cat}$ , where  $X$  is conversion of propane,  $F$  is flow rate in mol s<sup>-1</sup> and  $m_{cat}$  is the weight  
26 of the catalyst in g. Turnover frequencies were computed from this rate and the Brønsted acid site  
27 density determined by H/D exchange.  
28  
29  
30  
31  
32  
33  
34  
35  
36  
37  
38  
39  
40  
41  
42  
43  
44  
45

## 46 **3. Results**

### 47 *3.1. TMA CVD on AHFSY zeolite*

#### 48 *In situ FTIR characterization*

49  
50  
51  
52 The reaction of TMA with zeolitic BAS of dehydrated AHFSY was monitored by in situ FTIR  
53 spectroscopy. Fig. 1A shows the spectral changes in the OH and CH stretching regions upon  
54  
55  
56  
57  
58  
59  
60

exposure of AHFSY to TMA and subsequent treatment in H<sub>2</sub>. The introduction of TMA at 50°C (spectra a-b in Fig. 1) results in a nearly complete disappearance of all bands in the hydroxyl region including those associated with Brønsted acid sites (3549 and 3631 cm<sup>-1</sup>) in sodalite cages and faujasite supercage, respectively, as well as with silanol groups (3744 cm<sup>-1</sup>). This can be tentatively ascribed to the stoichiometric replacement of Brønsted acid sites and silanol groups at the external zeolite surface with Al(CH<sub>3</sub>)<sub>n</sub><sup>(3-n)+</sup> ions.<sup>63</sup>

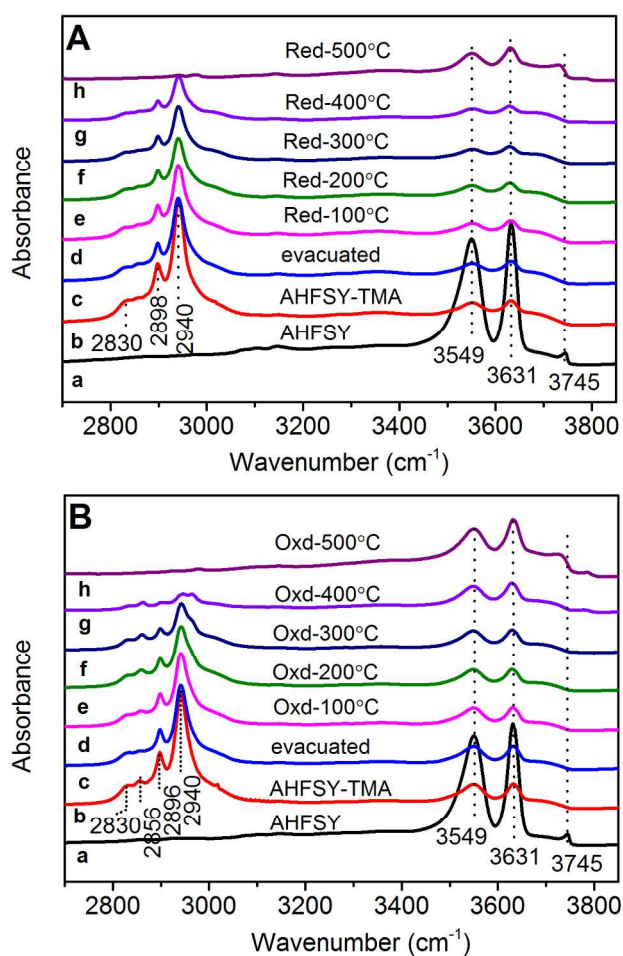


**Figure 1.** In situ FTIR spectra of the CVD of TMA onto AHFSY zeolite and the decomposition of the grafted organo-aluminum species via reduction (A) and oxidation (B). (a) Room temperature spectrum of the dehydrated parent AHFSY, (b) exposed to TMA, (c) evacuated for 20 min at 50 °C, followed by reduction in H<sub>2</sub> (A) or O<sub>2</sub> (B) (50 mbar) and subsequent evacuation at (d) 100 °C, (e) 200 °C, (f) 300 °C, (g) 400 °C, (h) 500 °C.

1  
2  
3 After TMA adsorption, the spectrum contains a set of bands in the region 2800-3000  $\text{cm}^{-1}$  due  
4 to C-H vibrations (*spectrum b* in Fig. 1 A and B). A small amount of BAS remains visible after  
5 prolonged exposure to TMA, which may be due to steric hindrances imposed by the cationic  
6 complexes. Upon reduction in static  $\text{H}_2$  (AHFSY-TMA-Red, 100-400 $^\circ\text{C}$ ) followed by  
7 evacuation (*spectra c-g*, Fig. 1 A) bands at 2940, 2898, 2865 and 2830  $\text{cm}^{-1}$  corresponding to  
8 symmetric and asymmetric C-H stretching of  $\text{CH}_3$  gradually decrease in intensity. Treatment  
9 with  $\text{H}_2$  at 500  $^\circ\text{C}$  is required to completely eliminate these bands. Concomitantly, it is seen that a  
10 small fraction of the original zeolitic BAS is regenerated. This regeneration becomes more  
11 prominent with increasing temperature. The nature of the charge-compensating Al species  
12 formed during the reaction with  $\text{H}_2$  is not clear. As in principle there is no external source of  
13 oxygen, it may on the one hand be suggested that reduction of the grafted organo-aluminum  
14 intermediates should result in aluminum hydride (Al-H) species, whose formation may indeed be  
15 surmised by observation of a very weak band around 1932  $\text{cm}^{-1}$  (supporting information, Fig.  
16 S1). The intensity of this band is the highest after exposing the AHFSY-TMA to  $\text{H}_2$  at 100 $^\circ\text{C}$ . It  
17 gradually decreases following reduction at higher temperatures and it is completely eliminated  
18 after treatment in  $\text{H}_2$  at 500  $^\circ\text{C}$ . On the other hand, as will be shown below by XRD and NMR,  
19 the reductive treatment leads also to the decomposition of the zeolite framework, abstraction of  
20 framework oxygen ions and formation of strong Si- $\text{CH}_3$  bonds, which can provide the oxygen  
21 species that are used to form extraframework Al-oxo complexes. Indeed, a weak band at 3778  
22  $\text{cm}^{-1}$  observed in the spectra of activated catalysts can be assigned to hydroxyl groups associated  
23 with the EFAl phase.<sup>64</sup>

24  
25  
26  
27  
28  
29  
30  
31  
32  
33  
34  
35  
36  
37  
38  
39  
40  
41  
42  
43  
44  
45  
46  
47  
48  
49  
50  
51  
52  
53  
54 An alternative procedure for the decomposition of the grafted cations in  $\text{O}_2$  atmosphere  
55 (AHFSY-TMA-Oxd) was also investigated. Upon oxidation at 100 and 200 $^\circ\text{C}$  (*spectra d and e* in  
56  
57  
58  
59  
60

1  
2  
3 Fig. 1 B), C-H stretching bands due to grafted TMA gradually decrease with the concomitant  
4 appearance of several new bands at intermediate temperatures. These bands are due to oxidation  
5 products of Al-CH<sub>3</sub> groups and oligomeric hydrocarbon species. These bands completely  
6 disappear after treatment in O<sub>2</sub> at 500 °C. The oxidation of the methyl groups results in carbon  
7 oxides and water. In the presence of water, the cationic Al species will hydrolyze, which will  
8 lead to regeneration of the BAS as well as further agglomeration of EFAl. Indeed, comparison of  
9 the IR spectra after H<sub>2</sub> and O<sub>2</sub> treatments evidences more pronounced regeneration of BAS for  
10 the latter treatment.  
11  
12  
13  
14  
15  
16  
17  
18  
19  
20  
21

22  
23 When the reduction treatment was followed by oxidation in O<sub>2</sub> at 500 °C (AHFSY-TMA-Red-  
24 Oxd), the FTIR spectrum (not shown) did not appreciably change. Nevertheless, one can expect  
25 that such a sequential activation procedure may lead to a more selective transformation of  
26 partially reduced and coordinatively unsaturated species formed upon the high-temperature  
27 reduction of AHFSY-TMA-red into more uniform AlO<sub>x</sub> structures than those formed upon the  
28 direct oxidative decomposition of AHFSY-TMA.  
29  
30  
31  
32  
33  
34  
35  
36  
37

#### 38 *Chemical composition, crystallinity, surface area and porosity*

39  
40 The X-ray powder diffraction patterns of as-synthesized AHFSY-TMA, AHFSY-TMA-Red,  
41 AHFSY-TMA-Oxd and AHFSY-TMA-Red-Oxd are shown in the supporting information (Fig.  
42 S2 A). The crystallinity of the zeolite after CVD of TMA (AHFSY-TMA) is close to 100%. It  
43 however strongly decreases after high-temperature activation. After decomposition of the grafted  
44 TMA, the crystallinity of the modified AHFSY zeolites is in the range 70-82% .  
45  
46  
47  
48  
49  
50  
51  
52  
53  
54  
55  
56  
57  
58  
59  
60



**Table 1.** Textural properties determined by Ar physisorption<sup>a</sup> and the chemical composition and unit cell dimensions ( $a_0$ ) of different faujasite catalysts as well as framework Al ( $Al_F$ ) density derived from XRD.

Sample	$c(Al)^{ICP}$ (mmol/g)	Al (wt%)	Si (wt%)	$a_0$ (Å)	$c(Al_F)^{XRD^b}$ (mmol/g)	$S_{BET}$ (m <sup>2</sup> /g)	$S_{micro}$ (m <sup>2</sup> /g)	$S_{meso}$ (m <sup>2</sup> /g)	$V_{micro}$ (cm <sup>3</sup> /g)	$V_{meso}$ (cm <sup>3</sup> /g)
AHFSY	2.9	7.8	n.d. <sup>c</sup>	24.536	3.25	539	468	70	0.21	0.09
-TMA-Hyd	3.9	10.6	34.5	24.460	2.42	383	332	51	0.15	0.09
-TMA-Red	3.0	8.2	30.9	24.369	1.436	391	305	86	0.15	0.12
-TMA-Oxd	3.2	8.6	31.4	24.353	1.248	317	256	61	0.13	0.08
-TMA-Red-Oxd	3.0	8.1	31.6	24.261	0.245	383	332	51	0.15	0.09

<sup>a</sup>  $S_{BET}$  – BET surface area;  $S_{micro}$  and  $S_{meso}$  – microporous and mesoporous surface areas, respectively;  $V_{micro}$  and  $V_{meso}$  – microporous and mesoporous pore volumes, respectively

<sup>b</sup> calculated from  $Al_F/U.C. = 107.1(a_0 - 24.238)^{14}$  under the assumption of a perfect zeolite framework with unit cell  $H_xSi_{192-x}Al_xO_{384}$  (i.e., without absorbed water and  $Al_{EF}$  species)

<sup>c</sup> Not determined

More pronounced are the changes in the lattice constant ( $a_0$ ) observed after the modification of AHFSY with TMA (Table 1). This parameter can be correlated to the density of framework Al ions in the zeolite.<sup>7</sup> The concentration of  $Al_F$  in AHFSY-TMA as determined by XRD is about 25% lower than that in parent AHFSY. Furthermore, the lattice Al content decreases upon the high-temperature activation (Table 1). The lowest estimated lattice Al content ( $C(Al_F)^{XRD}$ ) corresponding to the smallest unit cell size is for the catalyst activated in the reduction-oxidation cycle. Further evidence for strong dealumination of the faujasite framework upon reaction with TMA can be observed in the only slight increase of the total Al content in the modified zeolites ( $C(Al)^{ICP}$ , Table 1). Indeed, an almost complete substitution of BAS upon modification of

1  
2  
3 AHFSY with TMA has been observed by FTIR spectroscopy (Fig. 1). Even if one assumes  
4 substitution of every BAS with a monomeric  $\text{Al}(\text{CH}_3)_2^+$  ion, the Al and Si content in AHFSY-  
5 TMA should be ~ 14 and 33 wt. % . Whilst ICP analysis confirms the Si content, the Al content  
6 of the TMA-modified samples is significantly lower. This implies that the thermochemical  
7 activation results in loss of Al, which appears to be independent whether a reductive or oxidative  
8 treatment is employed. A word of caution is in place as the correlation for estimating  $c(\text{Al}_F)$  from  
9 XRD is valid for an intact zeolite framework. It can be expected that the interaction of TMA with  
10 the zeolite framework will not only remove part of the  $\text{Al}_F$  but also induce very strong local  
11 distortions in the lattice.  
12  
13  
14  
15  
16  
17  
18  
19  
20  
21  
22  
23

24  
25 The Ar physisorption data show that TMA-modified zeolites have a significantly lower BET  
26 surface area ( $S_{\text{BET}}$ ) than the parent zeolite (Table 1). This leads to a concomitant decrease of the  
27 micropore volume ( $V_{\text{micro}}$ ). The difference should be due to the inclusion of extraframework Al  
28 species in the zeolite. The lowest micropore surface area is observed for AHFSY-TMA-Oxd  
29 which may be traced back to the formation of significant amounts of water following oxidation  
30 of the methyl ligands in this case. However, the various treatments do not lead to the formation  
31 of significant amounts of mesopores as can be concluded from comparison of the mesopore  
32 surface areas and volumes. It implies that the structural modifications only occur at the local  
33 level.  
34  
35  
36  
37  
38  
39  
40  
41  
42  
43  
44  
45  
46

### 47 *3.1 NMR spectroscopy*

#### 48 *$^1\text{H}$ MAS NMR*

49  
50 To obtain better insight into the changes in AHFSY resulting from CVD of TMA, the  
51 materials were studied by solid-state magic angle spinning NMR spectroscopy. Representative  
52  $^1\text{H}$  NMR spectra of the parent AHFSY zeolite and the TMA-modified catalysts are shown in Fig.  
53  
54  
55  
56  
57  
58  
59  
60

1  
2  
3 2. In agreement with the FTIR data, CVD of TMA results in the disappearance of almost all  
4 zeolitic hydroxyl groups including the BAS located in the faujasite sodalite (4.56 ppm) and  
5 supercages (3.90 ppm). Also the peak due to silanol groups (1.90 ppm) disappears almost  
6 completely. At the same time, several new signals appear related to grafted alkylaluminum -  
7  
8  $\text{Al}(\text{CH}_3)_2$  species (broad signal between -0.3 and -0.8 ppm) and silane  $\text{O}_{4-n}\text{Si}(\text{CH}_3)_n$ <sup>63</sup> moieties  
9 (0.0-0.2 ppm, Fig. 2 (b)). The latter confirms the substantial structural modifications of the  
10 zeolite lattice. Subsequent reduction at 500 °C in  $\text{H}_2$  leads to decomposition of a major part of  
11 the alkylaluminum groups, whereas a substantial amount of the silane groups remain present in  
12 AHFSY-TMA-Red. The intensity increase of the signal around 0 ppm suggests that more silane  
13 moieties are formed due to the reaction of grafted  $-\text{Al}(\text{CH}_3)_2$  fragments with the lattice at  
14 elevated temperature. This is in line with the appearance of the T and D sites at  $\sim -60$  and  $\sim -20$   
15 ppm, respectively, in the <sup>29</sup>Si CPMAS spectrum of the reduced sample (Fig. S3). In addition, a  
16 signal at 4.4 ppm appears in the <sup>1</sup>H NMR spectrum of AHFSY-TMA-Red, which may  
17 correspond to either Al-H or strongly polarized BAS. This peak disappears after oxidation,  
18 whereas the signal due to the supercage BAS at 3.9 ppm does not change upon reduction or  
19 oxidation. Furthermore, high-temperature catalyst activation leads to a signal representing  
20 extraframework Al-OH species (2.6 ppm). Because formation of this feature is already observed  
21 after reduction in pure  $\text{H}_2$  (in other words in the absence of any external source of oxygen), it is  
22 taken as an indication that the oxygen atoms in such extraframework species originate from the  
23 lattice. Oxidation of the reduced catalyst in  $\text{O}_2$  at 500 °C leads to complete decomposition of the  
24 grafted  $\text{Al}(\text{CH}_3)_n$  and most  $\text{Si}-\text{CH}_3$  species. Instead, additional extraframework Al-OH hydroxyl  
25 moieties and silanol groups are formed (AHFSY-TMA-Red-Ox, Fig. 2 (d)).  
26  
27  
28  
29  
30  
31  
32  
33  
34  
35  
36  
37  
38  
39  
40  
41  
42  
43  
44  
45  
46  
47  
48  
49  
50  
51  
52  
53  
54  
55  
56  
57  
58  
59  
60

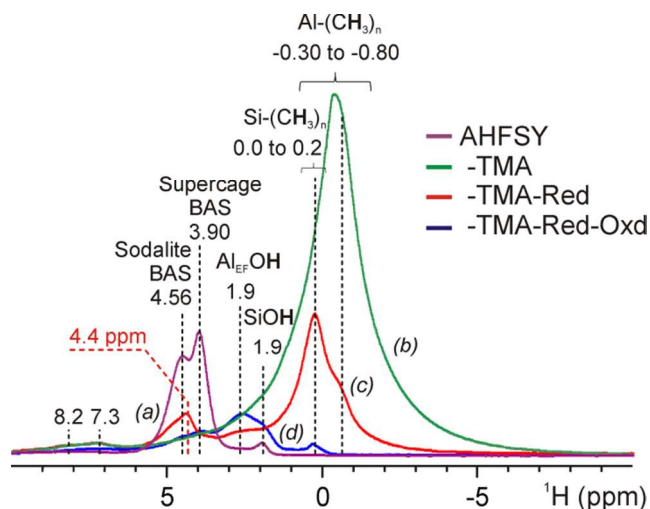


**Figure 2.**  $^1\text{H}$  NMR Hahn-echo spectra of (a) parent dehydrated AHFSY zeolite and (b) the material exposed to TMA (AHFSY-TMA) followed by (c) reduction in  $\text{H}_2$  at  $550^\circ\text{C}$  (AHFSY-TMA-Red) or (d) a sequential reduction in  $\text{H}_2$  and oxidation in  $\text{O}_2$  at  $550^\circ\text{C}$  (AHFSY-TMA-Red-Oxd).

We further analyzed the results of  $^1\text{H}\{-^{27}\text{Al}\}$  TRAPDOR (TRANSfer of Population in DOuble Resonance pulse sequence) NMR measurements. With  $^1\text{H}\{-^{27}\text{Al}\}$  TRAPDOR NMR one can identify protons located in the vicinity of Al centers.<sup>65,66</sup> The spectra for the reduced and oxidized AHFSY-TMA materials are presented in the supporting information Fig. S4. In the case of AHFSY-TMA-Red, signals of all protons including those from the silane ( $\text{Si-CH}_3$ ) moieties are affected by the Al irradiation. It is important to note that the signal at 4.4 ppm shows the same behavior with regards to the  $^{27}\text{Al}$  irradiation as the protons due to Al-bound hydroxyl groups. A more significant TRAPDOR effect is expected for the hydrogen atom directly bound to Al. This would suggest that this peak should be assigned to strongly polarized BAS rather than to aluminum hydride species. In principle, for specific geometries (regarding the angle between the  $^{27}\text{Al}\text{-}^1\text{H}$  dipole and  $^{27}\text{Al}$  quadrupole tensors) the TRAPDOR effect would also be weak. However, such specific geometries would be highly coincidental. Furthermore, the absence of aluminum hydride species is in line with the results of FTIR measurements showing that, although being formed upon hydrogenolysis of grafted TMA, Al-H species are not present in the

1  
2  
3 final reduced zeolite. The complete disappearance of this absorption band is observed after  
4  
5 reduction at 500 °C (Fig. S1).  
6

7  
8 After oxidation the behavior of  $^1\text{H}$  signals with respect to  $^{27}\text{Al}$  irradiation is substantially  
9  
10 changed (Fig. S4). For AHFSY-TMA-Red-Oxd, two different Si-CH<sub>3</sub> groups can be  
11  
12 distinguished characterized by signals at 0.20 ppm, which is sensitive to  $^{27}\text{Al}$  irradiation, and at 0  
13  
14 ppm, which is unaffected by  $^{27}\text{Al}$  irradiation. This suggests that these signals correspond to the  
15  
16 Si-CH<sub>3</sub> groups located in distinctly different chemical environments, most likely Al- and Si-rich  
17  
18 regions in the zeolite. The signal due to SiOH groups is hardly affected by the  $^{27}\text{Al}$  polarization,  
19  
20 suggesting that the regenerated silanol groups are located in Al-poor regions.  
21  
22  
23  
24  
25  
26

### 27 *$^{29}\text{Si}$ MAS NMR*

28  
29 We also investigated how the TMA modification influences the state of lattice silicon atoms.  
30  
31  $^{29}\text{Si}$  MAS NMR provides detailed information about the nature and coordination of the Si atoms.  
32  
33 In particular, it allows to estimate the framework Si/Al<sub>F</sub> ratio from the relative intensities of the  
34  
35  $^{29}\text{Si}$  NMR signals associated with Si atoms having different numbers of Al neighbors Q<sup>4</sup>(nAl),  
36  
37 where n stands for the number of Al neighbours.<sup>45, 67</sup>  
38  
39

40  
41 The direct-excitation (DE)  $^{29}\text{Si}$  MAS NMR spectrum of AHFSY is characterized by three  
42  
43 signals of the zeolite framework corresponding to silicon atoms surrounded by different number  
44  
45 of Al atoms, namely Si(2Al), Si(1Al) and Si(0Al) at chemical shift positions of -95, -101 and -  
46  
47 106 ppm, respectively (Fig. S3). The reaction with TMA (AHFSY-TMA) leads to a strong  
48  
49 decrease of the signals due to Q<sup>4</sup>(2Al) and Q<sup>4</sup>(1Al), whereas the signal attributed to Q<sup>4</sup>(0Al)  
50  
51 increases. This points to dealumination of the zeolite framework. In addition, a new signal at -  
52  
53 112 ppm occurs indicating the formation of regions with a high silica content. The DE spectra of  
54  
55 the reduced and the subsequently oxidized TMA-modified AHFSY differ only slightly in the  
56  
57  
58  
59  
60

1  
2  
3 intensities of Si(nAl) signals. The intensities of the different spectral components were obtained  
4  
5 by deconvolution of the DE  $^{29}\text{Si}$  MAS NMR spectra in terms of Gaussian line shapes using  
6  
7 DMfit2011.<sup>68</sup> The spectral deconvolution is shown in Fig. 3 and the relative intensities  $I_n$  of the  
8  
9 different  $\text{Q}^4(\text{nAl})$  signals summarized in Table 2, as well as the  $\text{Si}/\text{Al}_\text{F}$  values calculated by use of  
10  
11 the formula  $\text{Si}/\text{Al}_\text{F} = 4 (\sum I_n) / (\sum n I_n)$ .<sup>45, 67, 69</sup> In principle, the intensities  $I_1$  and  $I_2$  of  $\text{Q}^4(1\text{Al})$  and  
12  
13  $\text{Q}^4(2\text{Al})$  Si atoms at -101 and -95 ppm may also comprise contributions from silanol moieties  
14  
15  $\text{Q}^3(0\text{Al})$  and  $\text{Q}^3(1\text{Al})$  in the TMA-modified zeolite lattice. However, the gravimetric  $\text{Al}_\text{F}$   
16  
17 densities derived from the calculated  $\text{Si}/\text{Al}_\text{F}$  ratios agree generally well with the  $\text{Al}_\text{F}$   
18  
19 concentrations estimated from XRD (Table 4). Thus, despite the expected damage to the zeolite  
20  
21 lattice in TMA modified AHFSY, the silanol concentration is still relatively low compared to the  
22  
23 density of Si atoms with Al neighbors. An obvious exception is the AHFSY-TMA-Red-Oxd  
24  
25 case, where the value derived from the XRD lattice constant is much lower. This is probably  
26  
27 caused by the strong lattice distortions induced by the sequential reduction-oxidation treatment  
28  
29 of the TMA-containing AHFSY.  
30  
31  
32  
33  
34  
35

36 The overall  $^{29}\text{Si}$  NMR intensity can be greatly enhanced by using  $^1\text{H}$ - $^{29}\text{Si}$  cross-polarization  
37  
38 (CP) (Figs. S3B,C), but the resulting NMR spectra are generally not quantitative, because  
39  
40 proton-rich species tend to be relatively over-emphasized. Interestingly, in addition to the major  
41  
42  $\text{Q}^4(\text{nAl})$  signals already mentioned above (Fig. 3, Fig S3A), the CP-enhanced spectrum of  
43  
44 AHFSY-TMA-Red shows two broad signals around -60 ppm and -20 ppm, which are attributed  
45  
46 to T-sites ( $-\text{SiCH}_3$ ) and D-sites ( $-\text{Si}(\text{CH}_3)_2$ ), respectively, (Fig. S3C) formed during reduction.  
47  
48 High-temperature oxidation results in the decomposition of these silane moiety, as evidenced by  
49  
50 the disappearance of the T and D sites.  
51  
52  
53  
54  
55  
56  
57  
58  
59  
60

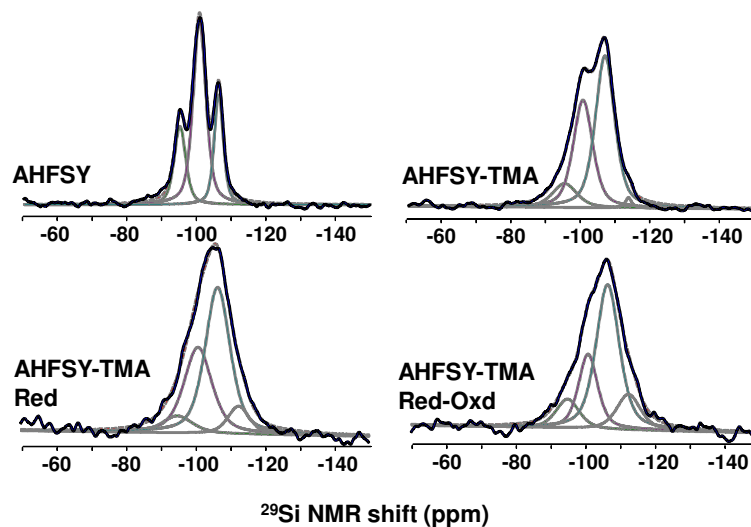


**Figure 3.** Deconvoluted direct-excitation  $^{29}\text{Si}$  MAS NMR spectra of AHFSY, AHFSY-TMA, AHFSY-TMA-Red and AHFSY-TMA-Red-Oxd. The relative intensities of different structure units and the calculated lattice Si/Al ratios are given in Table 2.

**Table 2** Relative intensities of the  $^{29}\text{Si}$  NMR signal components and calculated Si/Al<sub>F</sub> ratios for AHFSY and the as prepared (dehydrated) TMA-modified zeolites.

Samples	Si(2Al)	Si(1Al)	Si(0Al)	Si(0Al)	Si/Al <sub>F</sub> (NMR)
	(%)	(%)	(%)	(%)	
	-95 ppm	-101 ppm	-107 ppm	-112 ppm	
AHFSY	21	55	24	-	4.1
AHFSY-TMA	10	37	51	2	6.9
AHFSY-TMA-Red	7	33	51	9	8.4
AHFSY-TMA-Red-Oxd	11	23	53	13	9.0

### *<sup>27</sup>Al MAS and MQMAS NMR*

Aluminum atoms in perfect crystalline zeolite lattices such as in the parent AHFSY material are tetrahedrally coordinated and characterized by an isotropic <sup>27</sup>Al chemical shift ranging from 55 to 65 ppm (see Fig. S5). The introduction of extraframework species into the zeolite pores through chemical treatment or via dealumination of the lattice leads to more complex <sup>27</sup>Al MAS NMR spectra. The signal of tetrahedral Al becomes broader as a result of distortions in the oxygen-coordination symmetry around the Al atoms. Furthermore, the resolution and the <sup>27</sup>Al NMR visibility suffer from the second-order quadrupolar broadening, which is not completely eliminated by magic-angle spinning. In addition, the formation of octahedral and penta-coordinated Al<sup>EF</sup> leads to new signals at ~0 ppm and ~35 ppm, respectively, in <sup>27</sup>Al NMR spectra.

As generally observed for dehydrated zeolites,<sup>70</sup> the <sup>27</sup>Al NMR spectra of the as prepared TMA-modified zeolites samples are poorly resolved. They all contain an asymmetric broad peak at ~58 ppm (Figs. 4D and S5A), which is attributed to tetrahedral aluminum (Al<sub>F</sub><sup>IV</sup>). For AHFSY-TMA, the spectrum contains a number of overlapping spinning sideband patterns in the range from 200 ppm to -200 ppm, indicative of the heterogeneous Al speciation and strong quadrupolar interactions of framework and extraframework Al with distorted oxygen-coordination symmetry. Upon reduction (AHFSY-TMA-Red), the spectrum contains two overlapping resonances, one around 55 ppm and the other one around 35 ppm. The peaks broaden further upon oxidative treatment, suggesting an increase in the heterogeneity of the Al species.



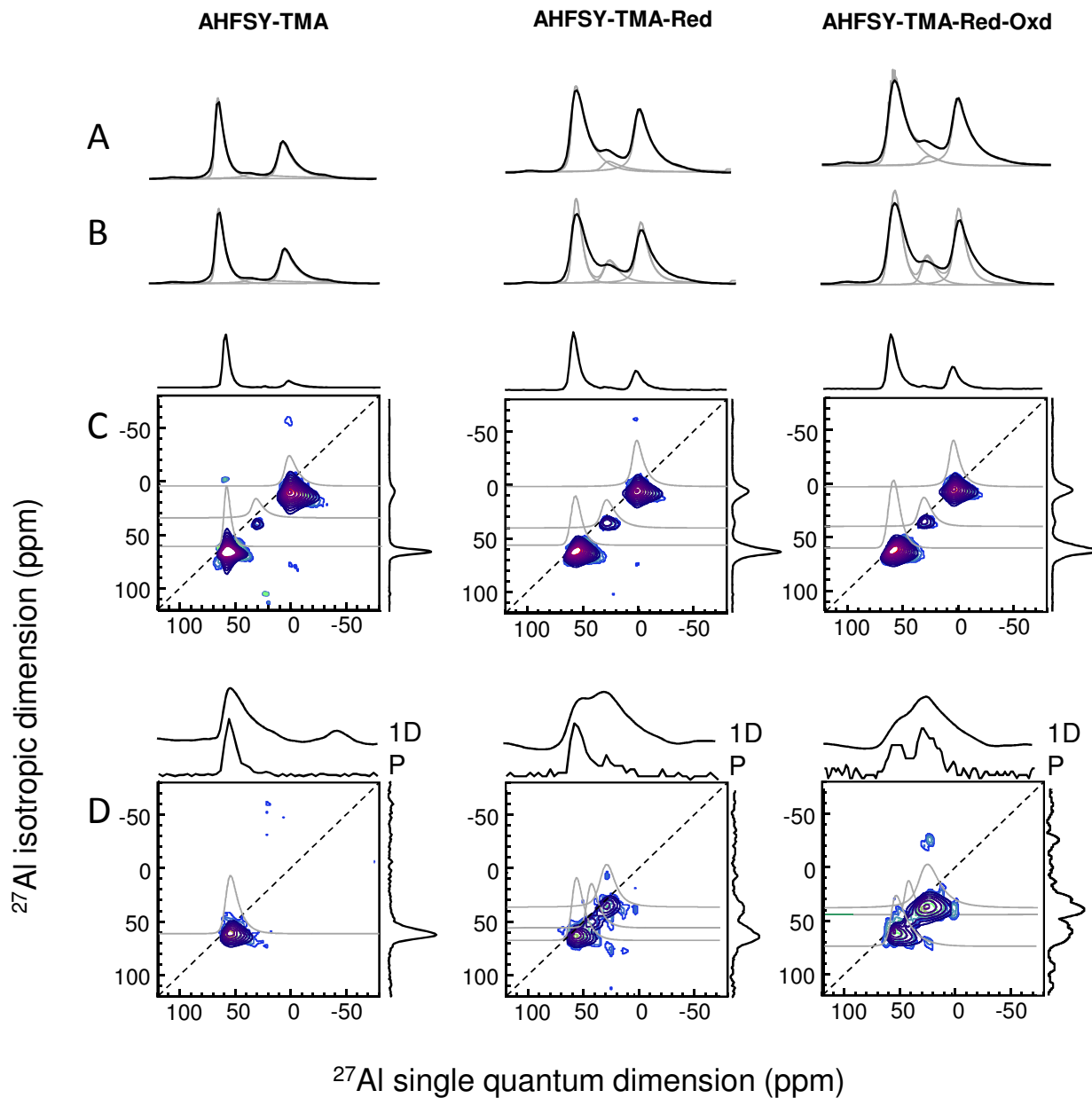


**Figure 4.**  $^{27}\text{Al}$  MAS NMR spectra of the TMA-modified zeolites. (A,B) 1D single-pulse-excitation spectra of air-exposed, hydrated samples analyzed in different ways (see below); (C,D) 2D MQMAS NMR spectra of (C) air-exposed hydrated zeolites and (D) the same materials in the dehydrated state before exposure to moist air. Projections (P) on the (horizontal) direct and (vertical) indirect frequency axis are indicated along the respective 2D spectra. Above the 2D spectra of the dehydrated samples in (D) the respective 1D spectra are also shown. All spectra were analyzed in terms of lineshape components involving Gaussian distributions of isotropic chemical shifts and quadrupolar coupling constants. The lineshape parameters resulting from spectral fitting are given in Table 3. For the lineshape deconvolution in (B) the same model as in (C) is used with only the signal-component heights as free fitting parameters. The 1D lineshape components predicted on the basis of the simulated MQMAS spectra are too narrow. The analysis of the 1D spectra in (A) is based on a less restricted lineshape fit with adjustable center  $C_Q$  and the width  $\Delta C_Q$  of the quadrupolar coupling constant distribution (Table 3).

1  
2  
3  
4  
5  
6 To get more detailed insight into the nature of Al species in modified zeolites, the multiple-  
7  
8 quantum magic angle spinning (MQMAS) NMR spectra were recorded. This technique offers  
9  
10 the possibility to separate the quadrupolar induced shift and broadening of the  $^{27}\text{Al}$  resonances  
11  
12 reflecting local electric field gradients around the Al atoms, on the one hand, and the isotropic  
13  
14 chemical shifts typical of the chemical structure around the Al atoms, such as the oxygen  
15  
16 coordination state, on the other hand. Chemical heterogeneity shows up as broadening along the  
17  
18 diagonal in the 2D spectrum, whereas the second-order quadrupolar effect is reflected by  
19  
20 broadening along the (horizontal) direct-frequency axis. In addition there is also a quadrupolar-  
21  
22 coupling effect on the signal positions. The stronger the quadrupolar coupling, the further the  
23  
24 resonances are separated from the spectral diagonal.<sup>67</sup> MQMAS spectra of the as-prepared,  
25  
26 dehydrated TMA-modified zeolites show indeed increased spectral resolution (Fig. 4D). Two  
27  
28 resonances with isotropic shifts ~58 and ~30 ppm can already be recognized by visual inspection  
29  
30 of the spectra of AHFSY-TMA-Red and AHFSY-TMA-Red-Oxd. The 58 ppm signal is  
31  
32 attributed to tetrahedral framework Al, and the 30 ppm signal to penta-coordinated  
33  
34 extraframework Al. Detailed lineshape simulation by use of “Czjzek” lineshape components  
35  
36 based on a Gaussian distribution of isotropic shifts and quadrupolar coupling constants<sup>68,71</sup>  
37  
38 reveals that there is a third signal around 45 ppm (Table 3). A signal at this position has  
39  
40 previously be assigned to tetrahedral extraframework Al.<sup>72</sup>  
41  
42  
43  
44  
45  
46  
47  
48  
49  
50  
51  
52  
53  
54  
55  
56  
57  
58  
59  
60

**Table 3:** Lineshape parameters\* of the signal components in  $^{27}\text{Al}$  MAS NMR spectra of the parent AHFSY and TMA-modified zeolites.

	Al site	$\delta_{\text{iso}}$ ( $\Delta\delta_{\text{iso}}$ ) (ppm)	$C_Q$ ( $\Delta C_Q$ ) (MHz)	$C'_Q$ ( $\Delta C'_Q$ ) (MHz)	fraction	$c(\text{Al}_F)$ mmol/g
<b>AHFSY</b>						
Hydrated	T	61 (5)	2.1 (1.2)	0.8 (0.5)	1	2.9
<b>AHFSY-TMA</b>						
dehydrated	T	59 (7)	3.9 (2.0)	-	-	-
hydrated	T	62 (7)	2.9 (1.1)	3.4 (2.0)	0.47	1.7
	P	35 (4)	3.6 (1.6)	8.0 (5.1)	0.15	0.5
	O	5 (5)	3.8 (1.8)	4.4 (2.6)	0.37	1.3
<b>AHFSY-TMA-Red</b>						
dehydrated	T <sub>1</sub>	59 (7)	3.9 (2.0)	-	-	-
	T <sub>2</sub>	45 (7)	3.9 (2.0)	-	-	-
	P	30 (10)	3.6 (1.6)	-	-	-
hydrated	T	61 (5)	3.3 (1.7)	4.7 (2.8)	0.48	1.7
	P	33 (6)	4.2 (2.0)	5.2 (2.9)	0.09	0.3
	O	5 (6)	3.4 (1.8)	4.5 (2.7)	0.43	1.5
<b>AHFSY-TMA-Oxd</b>						
Hydrated	T	63 (7)	3.8 (1.1)	5.0 (2.9)	0.41	1.3
	P	36 (8)	4.8 (1.6)	8.4 (5.6)	0.19	0.6
	O	7 (6)	4.0 (1.6)	5.0 (2.5)	0.	1.2
<b>AHFSY-TMA-Red-Oxd</b>						
dehydrated	T <sub>1</sub>	56 (7)	4.9 (1.8)	-	-	-
	T <sub>2</sub>	46 (7)	4.0 (1.3)	-	-	-
	P	30 (10)	4.8 (1.8)	-	-	-
hydrated	T	60 (8)	3.5 (1.6)	4.7 (4.1)	0.49	1.4
	P	33 (7)	4.0 (1.8)	5.1 (2.2)	0.06	0.2
	O	4 (6)	3.2 (1.7)	4.7 (3.1)	0.45	1.3

\*:  $\delta_{\text{iso}}$  : average isotropic chemical shift;  $\Delta\delta_{\text{iso}}$  : full-width-at-half-maximum (fwhm) of the Gaussian  $\delta_{\text{iso}}$  distribution;  $C_Q$ : average quadrupolar coupling constant;  $\Delta C_Q$ : fwhm of the Gaussian  $C_Q$  distribution.  $C_Q$  and  $\Delta C_Q$  determined from MQMAS spectra;  $C'_Q$ ,  $\Delta C'_Q$  and signal-intensity fractions determined from 1D  $^{27}\text{Al}$  NMR spectra of the hydrated zeolites;  $\text{Al}^{\text{IV}}$ ,  $\text{Al}^{\text{V}}$  and  $\text{Al}^{\text{VI}}$  densities from the intensity fractions and the total Al content  $c(\text{Al})_{\text{tot}}^{\text{Al NMR}}$  in Table 3. T: tetrahedral Al; P: pentacoordinated Al; O: octahedral Al.

1  
2  
3 The projections of the MQMAS spectra on the single-quantum frequency axis and the  
4 corresponding 1D single-pulse-excitation spectra are strongly different (indicated above the 2D  
5 spectra in Fig. 4D). As can be observed, only the (narrower) signals of  $^{27}\text{Al}$  spins with moderate  
6 quadrupolar coupling interactions show up in the MQMAS spectra recorded at 11.7 T. This is  
7 caused by the reduced triple-coherence generation for  $^{27}\text{Al}$  spins with quadrupolar coupling  
8 stronger than the radio-frequency fields employed for excitation. The MQMAS spectra thus  
9 reflect only part of the heterogeneous Al sites. One way to make MQMAS less selective and be  
10 able to detect (almost) all  $^{27}\text{Al}$  spins is to reduce the strong quadrupolar interactions by hydration  
11 of the zeolites. The presence of water molecules with their electrical dipoles decreases the local  
12 electronic field gradients around the  $^{27}\text{Al}$  nuclei. This results in weaker quadrupolar coupling  
13 interactions, causing less quadrupolar broadening and thus enhancing the chemical resolution in  
14  $^{27}\text{Al}$  MAS NMR. Unfortunately, for the TMA-modified AHFSY zeolites it will also significantly  
15 alter the chemical environment of the Al centers. Nevertheless, if the effect of water and air is  
16 taken into account,  $^{27}\text{Al}$  NMR of the hydrated TMA-modified zeolites may still give  
17 ‘retrospective’ insight into structures formed and the lattice damage resulting from TMA  
18 deposition and consequent high-temperature treatments with hydrogen and oxygen.  
19  
20  
21  
22  
23  
24  
25  
26  
27  
28  
29  
30  
31  
32  
33  
34  
35  
36  
37  
38  
39

40  
41 1D and 2D  $^{27}\text{Al}$  NMR spectra of the hydrated TMA-modified samples indeed show much  
42 better resolved signals attributed octahedral, penta-coordinated and tetrahedral Al atoms at ~5,  
43 ~33 and ~61 ppm, respectively (Figs, 4A-C). The relative amount of octahedral Al increases  
44 upon hydrogen and oxygen treatment. This trend correlates with the appearance of penta-  
45 coordinated Al in as-prepared dehydrated AHFSY-TMA-Red and AHFSY-TMA-Red-Oxd (1D  
46 NMR spectra in Fig. 4D). This suggests that hydration causes conversion from originally penta-  
47 coordinated Al into octahedral Al species. Water molecules probably bind to under-coordinated  
48  
49  
50  
51  
52  
53  
54  
55  
56  
57  
58  
59  
60

1  
2  
3 Al centers. The absolute intensity of the tetrahedral Al signal of the parent AHFSY zeolite is  
4  
5 lower than those of the TMA-modified zeolites (Fig. S5B). This suggests that grafting of TMA  
6  
7 leads to dealumination of the faujasite framework, which would also be in line with the breakage  
8  
9 of the zeolite lattice reflected in  $^{29}\text{Si}$  NMR spectra (formation of D and T type silicon).  
10  
11 Therefore, the octahedral ( $\text{Al}_{\text{EF}}^{\text{VI}}$ ) and pentacoordinated ( $\text{Al}_{\text{EF}}^{\text{V}}$ ) Al species may not be  
12  
13 exclusively related to the additional Al atoms from TMA, but may also arise from the partial  
14  
15 framework dealumination and/or severe structural distortions of the originally tetrahedral lattice  
16  
17  $\text{Al}_{\text{F}}^{\text{IV}}$  sites. Subsequent high-temperature reduction and oxidation treatments lead to a further  
18  
19 decrease of the signal at 62 ppm belonging to tetrahedral Al sites and an increase of those  
20  
21 attributed to more coordinatively saturated extraframework species. In the chemical vapor  
22  
23 deposition procedure the initial TMA dose is much higher than the available Brønsted sites for  
24  
25 charge compensation. So, that it is likely that a fraction of EFAl exists as oligomeric oxygenated  
26  
27 Al clusters or even aggregated aluminum oxide species.  
28  
29  
30  
31  
32  
33

34 To quantitatively analyze the 1D  $^{27}\text{Al}$  NMR spectra of the hydrated zeolites in terms of  $\text{Al}^{\text{IV}}$ ,  
35  
36  $\text{Al}^{\text{V}}$  and  $\text{Al}^{\text{VI}}$  a proper lineshape model is required, which is not trivial due to the spectral overlap  
37  
38 and the asymmetric character of the second-order quadrupolar linebroadening. Therefore, the  
39  
40 individual lineshape parameters were first determined from MQMAS NMR spectra, because of  
41  
42 the lower signal overlap in the 2D spectra, and because of the additional information content in  
43  
44 the exact shift position (separation from the spectrum diagonal) and lineshape (horizontal /  
45  
46 diagonal line broadening) of the resonances. Deconvolution of these spectra in terms of the  
47  
48 earlier mentioned Czjzek components are summarized in Table 3. However, MQMAS spectra  
49  
50 are not quantitative in the sense that the signal intensities do not directly reflect the relative  
51  
52 occurrence of the various Al types in the material. Therefore, the MQMAS models were fitted  
53  
54  
55  
56  
57  
58  
59  
60

1  
2  
3 with minimal changes to the 1D single-pulse excitation spectra, which are quantitative, but suffer  
4 from higher signal overlap. First, all lineshape parameters, except the signal heights, were kept  
5 fixed in the analysis. This resulted in a quite reasonable fit to the 1D spectra, but the lineshape  
6 components extracted from the MQMAS spectra are too narrow for the 1D spectra (Fig. 4B).  
7  
8 Apparently, even after hydration, part of the Al with stronger quadrupolar couplings is under-  
9 represented in MQMAS. A better spectral fit results if the Gaussian-distribution center and width  
10 of the quadrupolar coupling constants  $C_Q$  and  $\Delta C_Q$  is allowed to change. In general, the overall  
11  $C_Q$  and  $\Delta C_Q$  values increase compared to those in the MQMAS spectra.

12  
13 If  $^{27}\text{Al}$  NMR visibility in the hydrated parent and TMA-modified zeolites is similar, the  
14 (weight-normalized) peak area of the central-transition frequency region in the respective  $^{27}\text{Al}$   
15 NMR spectra should be proportional to the total Al concentration measured by ICP,  $c(\text{Al})_{\text{total}}^{\text{ICP}}$ ,  
16 which is roughly the case (Table 4). The slightly lower values from NMR for hydrated AHFSY-  
17 TMA, AHFSY-TMA-Oxd and AHFSY-Red-Oxd indicate that a small Al fraction is NMR  
18 invisible as a result of low coordination symmetry. From the total Al content and the relative  
19 signal intensities for the  $\text{Al}^{\text{IV}}$ ,  $\text{Al}^{\text{V}}$  and  $\text{Al}^{\text{VI}}$  species obtained from the deconvolution of the 1D  
20 NMR spectra (Fig. 4A), the individual content of the different Al species can be calculated  
21 (Table 3). The  $\text{Al}^{\text{IV}}$  densities from  $^{27}\text{Al}$  NMR,  $c(\text{Al}_F)^{\text{Al NMR}}$ , correlate reasonably with the  $\text{Al}_F$   
22 densities from  $^{29}\text{Si}$  NMR ( $c(\text{Al}_F)^{\text{Si NMR}}$ ) and XRD ( $c(\text{Al}_F)^{\text{XRD}}$ ) (Table 4), but are systematically  
23 lower. This is the case, even for AHFSY, where  $^{27}\text{Al}$  NMR visibility should not be an issue. A  
24 likely explanation is that  $c(\text{Al}_F)^{\text{Al NMR}}$  is indirectly calibrated with respect to the ICP value for  
25 hydrated AHFSY, thus including adsorbed water. In contrast,  $c(\text{Al}_F)^{\text{Si NMR}}$  and  $c(\text{Al}_F)^{\text{XRD}}$  are  
26 specified per gram zeolite *lattice framework*, excluding extraframework species.

**Table 4.** Total Al concentrations from ICP ( $c(\text{Al})_{\text{tot}}^{\text{ICP}}$ ) and  $^{27}\text{Al}$  NMR ( $c(\text{Al})_{\text{tot}}^{\text{Al NMR}}$ ), and framework Al concentration from  $^{27}\text{Al}$  NMR ( $c(\text{Al}_F)^{\text{Al NMR}}$ ),  $^{29}\text{Si}$  NMR ( $c(\text{Al}_F)^{\text{Si NMR}}$ ) and XRD ( $c(\text{Al}_F)^{\text{XRD}}$ ).

Sample	$c(\text{Al})_{\text{tot}}^{\text{ICP}}$ (mmol/g)	$c(\text{Al})_{\text{tot}}^{\text{Al NMR}}$ (mmol/g) <sup>a</sup>	$c(\text{Al}_F)^{\text{Al NMR}}$ (mmol/g) <sup>b</sup>	$c(\text{Al}_F)^{\text{Si NMR}}$ (mmol/g) <sup>c</sup>	$c(\text{Al}_F)^{\text{XRD}}$ (mmol/g) <sup>d</sup>
AHFSY	2.9	2.9	2.9	3.2	3.25
AHFSY-TMA	3.9	3.5	1.7	2.3	2.42
AHFSY-TMA-Red	3.0	3.5	1.7	1.5	1.44
AHFSY-TMA-Oxd	3.2	3.1	1.3	1.5	1.25
AHFSY-TMA-Red-Oxd	3.0	2.9	1.4	1.9	0.46

<sup>a</sup> from total  $^{27}\text{Al}$  NMR peak area [120, -80 ppm] of hydrated TMA-modified AHFSY zeolites relative to AHFSY with 2.9 mmol/g Al (ICP value); <sup>b</sup> from relative intensity of the  $\text{Al}^{\text{IV}}$  signal of hydrated samples (Table 3) combined with  $c(\text{Al})_{\text{tot}}^{\text{Al NMR}}$ ; <sup>c</sup> framework Al density from the Si/Al ratio derived from  $^{29}\text{Si}$  NMR (Table 2) combined with 16.7 mmol T atoms / g zeolite *framework*; <sup>d</sup>  $c(\text{Al}_F)^{\text{XRD}} = 10.79 (a_0 - 24.238)$  with  $a_0$  the lattice constant (Å) assuming a unit cell  $\text{H}_x\text{Si}_{192-x}\text{Al}_x\text{O}_{384}$ .

### 3.3. Brønsted and Lewis acidity

#### *H/D exchange with perdeuterated benzene*

Selective H/D exchange of perdeuterated benzene with zeolitic BAS was monitored by FTIR spectroscopy in order to investigate the effect of TMA-modification on the intrinsic acidity of AHFSY zeolites. After the decomposition of grafted TMA under reducing condition at high temperature and prior to reaction with  $\text{C}_6\text{D}_6$ , the OH stretching region of TMA-AHFSY-Red zeolite contains two absorption bands with maxima at 3549 and 3631  $\text{cm}^{-1}$  corresponding to the BAS located in faujasite sodalite cages and supercages, respectively (Fig. 5). Upon reaction with  $\text{C}_6\text{D}_6$ , the intensity of these bands gradually decreases, while new bands appear in the OD stretching region (Fig 5 A, right panel). Most of the BAS in AHFSY-TMA-Red react with  $\text{C}_6\text{D}_6$

1  
2  
3 already after prolonged contact at 30 °C. Deuteration is nearly complete after reaction at 100 °C.  
4  
5 The total acidity of AHFSY-TMA-Red is 0.3 mmol/g (Table 5), amounting to 10% of the total  
6  
7 number of acid sites in AHFSY.  
8  
9

10  
11  
12 **Table 5.** Initial C<sub>6</sub>D<sub>6</sub> H/D exchange rates ( $k_{H/D}$ ) at 303K and total acidity ( $c(\text{BAS})^{\text{FTIR}}$ ) of  
13  
14 different faujasite catalysts.  
15  
16

17 18 19 Sample	$k_{H/D}$ (h <sup>-1</sup> )	$c(\text{BAS})^{\text{FTIR}}$ (mmol/g) <sup>a</sup>
20 21 22 AHFSY	1.1	3.3
23 24 25 AHFSY-TMA-Red	1.1	0.3
26 27 28 AHFSY-TMA-Oxd	0.3	0.7
29 30 31 AHFSY-TMA-Red-Oxd	0.4	0.7
32 33 34 USY-8	4.7	1.3

35  
36  
37 <sup>a</sup> – total concentration of BAS determined by the H/D exchange of C<sub>6</sub>D<sub>6</sub>  
38  
39

40  
41 The reaction of the oxygen-treated AHFSY-TMA zeolite with C<sub>6</sub>D<sub>6</sub> is much slower (Fig. 5 B).  
42  
43 In this case only a small fraction of BAS can be exchanged at 30 °C. The H/D exchange remains  
44  
45 slow at a temperature of 50 °C. Despite an apparent lower intrinsic acidity, the concentration of  
46  
47 BAS in AHFSY-TMA-Oxd (0.76 mmol/g) is approximately twice higher than in its reduced  
48  
49 counterpart. The exchange behavior and the total number of exchangeable BAS in the AHFSY-  
50  
51 Red-Oxd are very similar to that in AHFSY-TMA-Oxd (Table 5).  
52  
53  
54  
55  
56  
57  
58  
59  
60



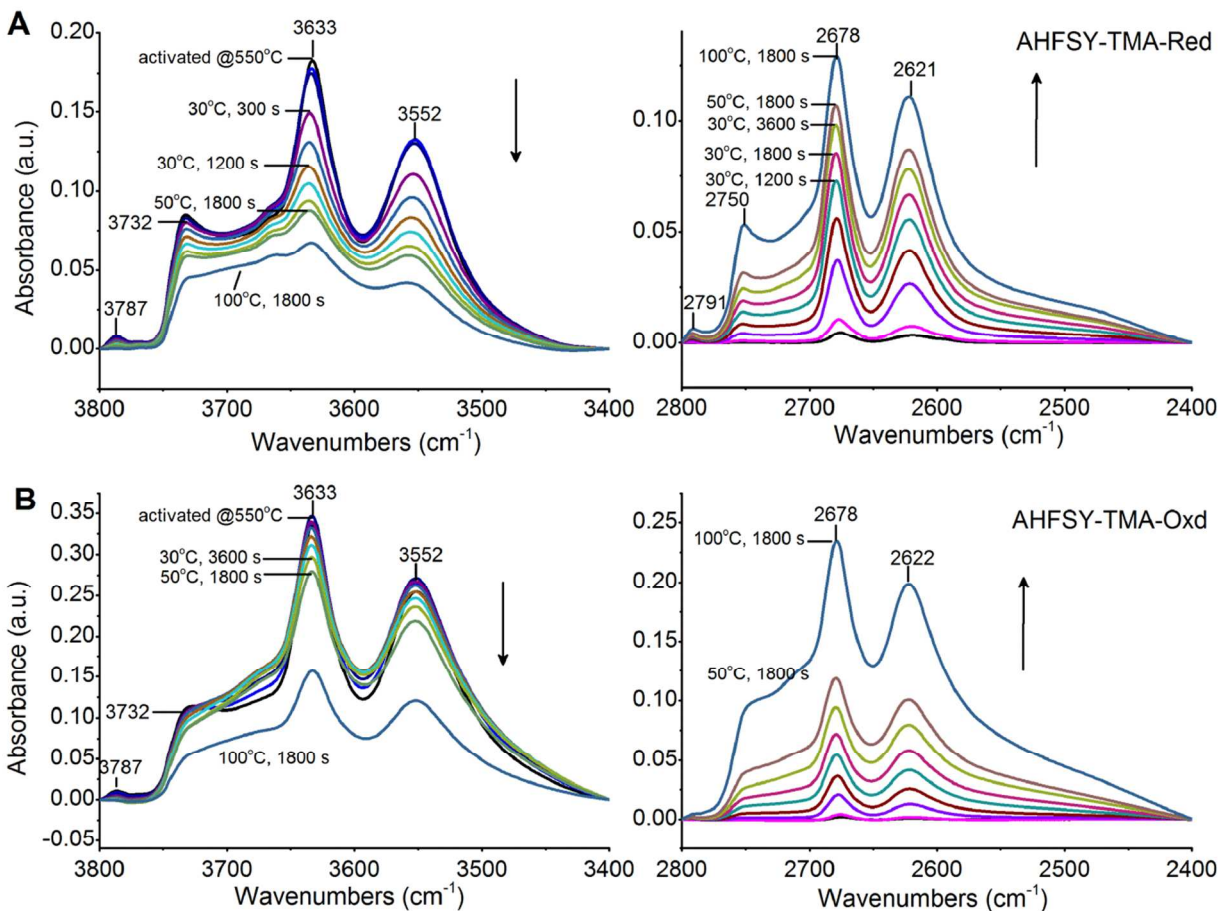


**Figure 5.** FTIR spectra of dehydrated AHFSY-TMA-Red (A) and AHFSY-TMA-Oxd (B) zeolites prepared in the regions of OH (left) and OD (right) stretching vibrations before and after reaction with  $C_6D_6$  with increasing exposure times at 30 °C followed by the gradual increase of the reaction temperature to 100 °C.

The intrinsic acidity of the modified zeolites can be compared by analyzing the rate of appearance rate of OD stretching vibrations in the FTIR spectra (Fig. 6). The first-order rate constants are given in Table 5. The initial H/D exchange rate for the TMA-modified AHFSY zeolite activated in  $H_2$  (AHFSY-TMA-Red) is similar to that of the original EFAl-free AHFSY zeolite. At higher exchange levels, the rate decreases. This may point to some heterogeneity in the strength of the BAS. However, the samples activated by high-temperature oxidation (AHFSY-TMA-Oxd and AHFSY-TMA-Red-Oxd) are clearly substantially less active in the H/D

exchange reaction (Fig. 6, Table 5). Noteworthy is also that the rates for the TMA-modified zeolites are much lower than those of EFAl-containing zeolites prepared by ion exchange but similar to the EFAl-containing zeolites prepared via incipient wetness impregnation.<sup>35</sup> The decreased intrinsic acidity of TMA-modified zeolites is surprising taking into account the pronounced dealumination of the zeolite framework in these materials (see section 3.2).

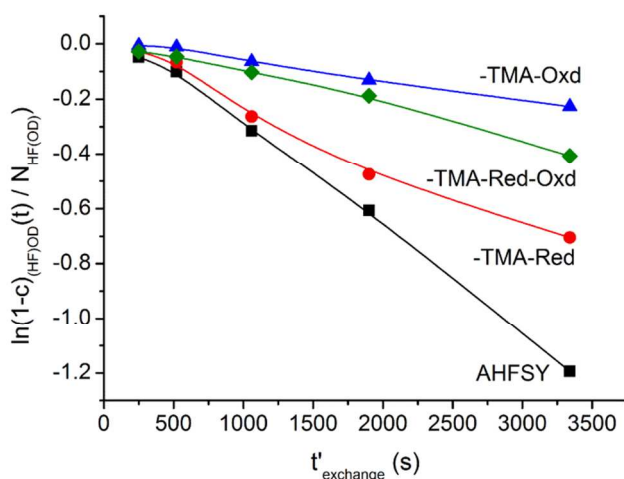


**Figure 6.** First-order plot of the rate of appearance of the band at ca.  $2680\text{ cm}^{-1}$  due to acidic deuteroxyl groups in the faujasite supercage upon reacting the parent AHFSY and TMA-modified zeolites with  $\text{C}_6\text{D}_6$ .  $c_{(\text{HF})\text{OD}}$  is the concentration of the respective OD groups at a particular stage of the H/D exchange at  $30^\circ\text{C}$ ,  $N_{(\text{HF})\text{OD}}$  is the total density of acid sites,  $t'_{\text{exchange}}$  is the exposure time to  $\text{C}_6\text{D}_6$ .

### *Infrared spectroscopy of adsorbed CO*

The presence and strength of the Lewis and Brønsted acid sites in TMA-modified faujasites was further probed by FTIR spectroscopy of CO adsorption at liquid nitrogen temperature. Both the perturbations of adsorbed CO and those of the zeolitic hydroxyl groups due to hydrogen bonding with CO molecules were monitored. The FTIR spectra in the region of OH and CO stretching vibrations ( $\nu(\text{OH})$  and  $\nu(\text{CO})$ , respectively) at increasing CO coverage for the TMA-modified zeolites are collected in the supporting information (Fig. S6). The red shifts of  $\nu(\text{OH})$  (denoted as  $\Delta\nu(\text{OH})$ ) are summarized in Table 6. The spectra of adsorbed CO are characterized

by  $\nu(\text{CO}) = 2177 \text{ cm}^{-1}$ . Both  $\nu(\text{CO})$  and  $\Delta\nu(\text{OH})$  are very similar for all zeolites. The red shift is slightly higher for the modified zeolites than for the EFAI-free AHFSY (Table 6).

**Table 6.** Positions of  $\nu(\text{CO})$  and  $\nu(\text{OH})$  stretching bands for  $\text{OH}\cdots\text{CO}$  complexes formed after adsorption of CO on zeolite catalysts at the liquid nitrogen temperature (shifts are with respect to the vibration of the hydroxyl groups in the supercages).

Catalyst	$\nu(\text{CO})$ ( $\text{cm}^{-1}$ )	$\nu(\text{OH})$ ( $\text{cm}^{-1}$ )	$\Delta\nu(\text{OH})$ ( $\text{cm}^{-1}$ )
AHFSY	2177	3338	294
AHFSY-TMA-Red	2177	3329	300
AHFSY-TMA-Oxd	2176	3332	301
AHFSY-TMA-Red-Oxd	2176	3329	300

### 3.4 Catalytic reactivity

The catalytic activity data including the overall reaction rate ( $r$ ), the rates of propane dehydrogenation to  $\text{H}_2$  and propylene ( $r^{\text{DEH}}$ ) and of propane cracking to ethylene and methane ( $r^{\text{CRC}}$ ) as well as turnover frequencies are collected in Table 7. In all cases, the catalytic activity was stable during the catalytic runs (Fig. S7). The overall conversion rate of the TMA-modified zeolites depends strongly on the pretreatment. The rate for AHFSY-TMA-Red is twice as high as the rate for the parent zeolite. It is even higher than the activity of the commercial steam-calcined USY-8 zeolite. After oxidation of this sample (AHFSY-TMA-Red-Oxd) the activity is lower than the parent zeolite. The activity of AHFSY-TMA-Oxd is close to that of AHFSY. The carbon-containing products from propane conversion under these conditions are methane,

1  
2  
3 ethylene and propylene. For the parent zeolite AHFSY, the rate of propane cracking with  
4 methane and ethylene as main products is much higher than the rate of propane dehydrogenation.  
5  
6 The contribution of cracking to propane conversion (CRC) is 82%. Upon modification by TMA  
7  
8 and reduction, the rate of propane dehydrogenation increases nearly 6 times, whilst the rate of  
9  
10 cracking only increases slightly. As a result, the contribution of propane cracking for this zeolite  
11  
12 has decreased to 48%. For AHSY-TMA-Oxd, this contribution is even lower, which is due to the  
13  
14 decreased (increased) rate of cracking (dehydrogenation) compared to the parent zeolite. Note  
15  
16 that the increase in dehydrogenation is less than for AHFSY-TMA-Red. When the reduced  
17  
18 zeolite is oxidized (AHFSY-TMA-Red-Oxd), the rates of propane cracking and dehydrogenation  
19  
20 decrease strongly, the latter more pronouncedly than the former so that the contribution of  
21  
22 cracking increases to 66%. Notably, the rate of propane cracking over USY-8 is almost as high  
23  
24 as that of AHFSY-TMA-Red, whilst its dehydrogenation activity is close to that of AHFSY-  
25  
26 TMA-Oxd. Except for AHFSY-TMA-Red, in all cases the molar methane-to-ethylene ratio was  
27  
28 very close to unity. It is 1.29 for AHFSY-TMA-Red indicating that the ethylene product is  
29  
30 further converted. Indeed, this is the only zeolite for which the formation of a small amount of  
31  
32 benzene was observed. The benzene selectivity was, however, below 1%. This may suggest that  
33  
34 also some coke formation takes place which did not lead to catalyst deactivation at the time scale  
35  
36 of the reaction test.  
37  
38  
39  
40  
41  
42  
43  
44

45 Table 7 also contains the turnover frequencies (TOF) for propane cracking and  
46  
47 dehydrogenation. These TOF values were computed on the basis of the BAS densities  
48  
49 determined by the H/D exchange method. The TOF for propane cracking of AHFSY-TMA-Red  
50  
51 is an order of magnitude higher than that of the parent zeolite and about 4 times higher than that  
52  
53 of USY-8. The TOF for propane dehydrogenation is also much higher for AFHSY-TMA-Red  
54  
55  
56  
57  
58  
59  
60

than for the two reference cases. The TOFs for cracking and dehydrogenation of the oxidized TMA-modified zeolites are substantially lower than the respective values for their reduced counterpart.

**Table 7.** Catalytic conversion of propane over TMA-modified AHFSY catalysts and commercial USY zeolite (WHSV = 11.7 h<sup>-1</sup>; T = 590 °C).

Sample	c(BAS) <sup>FTIR</sup> (mmol/g)	$r \times 10^{-5}$ (mol/g·s)	$r^{CRC} \times 10^{-5}$ (mol/g·s) <sup>a</sup>	$r^{DEH} \times 10^{-5}$ (mol/g·s) <sup>b</sup>	CRC (%)	TOF <sup>CRC</sup> (10 <sup>-3</sup> s <sup>-1</sup> ) <sup>d</sup>	TOF <sup>DEH</sup> (10 <sup>-3</sup> s <sup>-1</sup> ) <sup>e</sup>
AHFSY	3.34	14.8	11.8	2.6	82	35	7.8
-TMA-Red	0.34	29	14	15	48	412	441
-TMA-Oxd	0.73	17	6.9	9.8	41	95	134
-TMA-Red-Oxd	0.73	9	5.9	3.1	66	80	42
USY-8	1.29	21	13	8.5	60	101	66

#### 4. Discussion

The in situ FTIR data show that BAS of dealuminated zeolite Y can be made to react with TMA. Grafting of TMA onto the zeolite leads to complete removal of all hydroxyls, including the silanol and bridging hydroxyl groups. The resulting organometallic intermediates can be decomposed by treatment in oxygen or hydrogen atmosphere at elevated temperature. The IR spectra of TMA-modified zeolites differ substantially with respect to the way the grafted organoaluminum species are treated. The spectra contain indications that their hydrogenolysis in

1  
2  
3 H<sub>2</sub> results in the formation of Al-H species characterized by a weak band at around 1932 cm<sup>-1</sup> at  
4  
5 intermediate reduction temperature. At the highest temperature, these species and all methyl  
6  
7 groups have been reacted away. These changes go together with partial regeneration of the  
8  
9 zeolitic BAS in AHFSY-TMA-Red. The amount of Al deposited during CVD of TMA (cf.  
10  
11 AHFSY-TMA-Hyd in Table 1) corresponds to approximately 1/3 of the number of BAS initially  
12  
13 present. This suggests that the organometallic precursor undergoes multiple reactions with the  
14  
15 hydroxyl groups of the zeolite. As the Al content of AHFSY-TMA-Red is found to be lower than  
16  
17 that of the hydrated zeolite, it can be inferred that part of the deposited Al species has been  
18  
19 removed during reduction. Combined with the observation of the transient formation of Al-  
20  
21 hydride species, it may be speculated that during the high-temperature treatment volatile (AlH<sub>3</sub>)<sub>n</sub>  
22  
23 has been formed. The existence of such compounds has recently been reported.<sup>73</sup> In support of  
24  
25 this, it was observed that downstream the zeolite bed in the quartz reactor used for in situ  
26  
27 reduction a white powder was formed. This is likely due to the reaction of volatile aluminum  
28  
29 hydride species with hydroxyl groups of the surface of the quartz reactor. The oxidative  
30  
31 decomposition of the grafted organoaluminum species (AHFSY-TMA-Oxd) results in water and  
32  
33 carbon oxides. In the presence of water the Al-O bonds are hydrolyzed, as follows from the  
34  
35 much more pronounced regeneration of zeolitic BAS following oxidation compared to reduction.  
36  
37 Notably, in this case the Al content also decreases during the treatment.  
38  
39  
40  
41  
42  
43  
44  
45

46 The intensive reaction of TMA with more than one BAS results in significant distortions of the  
47  
48 zeolite lattice as follows from XRD and Ar physisorption measurements. MAS NMR confirms  
49  
50 the partial decomposition and dealumination of the framework. <sup>1</sup>H NMR shows that during CVD  
51  
52 of TMA nearly all zeolite hydroxyl groups are consumed. Concomitantly, Al-CH<sub>3</sub> and Si-CH<sub>3</sub>  
53  
54 species are formed. Thus, it can be inferred that CVD does not proceed by simple reactions as  
55  
56  
57  
58  
59  
60

1  
2  
3 encountered earlier for CVD of  $\text{Zn}(\text{CH}_3)_2$  onto high-silica ZSM-5 zeolite,<sup>39</sup> involving formation  
4 of  $\text{Zn}(\text{CH}_3)^+$  and methane. Besides reaction with the BAS, TMA will also attack Al-O-Si  
5 framework moieties. As Si- $\text{CH}_3$  bonds are stronger than Al- $\text{CH}_3$  bonds, it is likely that the  
6 rupture of the relatively weak framework bonds around the bridging hydroxyl group leads to Si-  
7  $\text{CH}_3$  and Al-O-{TMA} species. This is consistent with NMR and IR spectroscopic data. High-  
8 temperature treatment of AHFSY-TMA in  $\text{H}_2$  results in the decomposition of the Al- $\text{CH}_3$   
9 species, whilst the Si- $\text{CH}_3$  moieties remain intact. The latter are only decomposed when oxidized  
10 at 500 °C in  $\text{O}_2$  resulting in silanol groups. After reduction as well as after subsequent oxidation,  
11 a small portion of BAS is regenerated. Their regeneration is however stronger during the direct  
12 oxidative treatment. The nature of the regenerated protons depends on the activation method.  
13 The protons in AHFSY-TMA-Red give rise to an unusual resonance at 4.4 ppm in the  $^1\text{H}$  NMR  
14 spectrum. These are tentatively assigned to strongly polarized protons in the supercages. We  
15 propose that the polarization is caused by the interaction with neighboring Lewis acidic  
16 extraframework Al species. These protons were not observed anymore after oxidation of the  
17 zeolite sample. In such case,  $^1\text{H}$  resonances characteristic for faujasite zeolites were observed  
18 again. The decomposition of the intermediate silane species and the dealumination of the zeolite  
19 framework follows from the  $^{29}\text{Si}$  and  $^{27}\text{Al}$  NMR data. The  $^{27}\text{Al}$  NMR data also inform us about  
20 the fate of Al species. After reductive treatment of grafted TMA species, the Al species are  
21 mainly 4- and 5-coordinated. Oxidation of these species leads to a more heterogeneous Al  
22 speciation. From the strong quadrupolar broadening of the signals in the  $^{27}\text{Al}$  NMR spectra of  
23 dehydrated materials, it can be concluded that a substantial fraction of Al cannot be detected by  
24 NMR spectroscopy. Although this problem can be partially avoided by hydrating the zeolite  
25 samples, this procedure strongly alters the chemical environment of Al sites of the TMA-  
26  
27  
28  
29  
30  
31  
32  
33  
34  
35  
36  
37  
38  
39  
40  
41  
42  
43  
44  
45  
46  
47  
48  
49  
50  
51  
52  
53  
54  
55  
56  
57  
58  
59  
60

1  
2  
3 modified zeolites. The important corollary of the NMR results appears to be that dealumination  
4 occurs upon CVD of TMA. This is consistent with the lower concentration of framework Al<sup>IV</sup>  
5 species derived from XRD analysis. Based on the IR, XRD and NMR results, it can be  
6 concluded that the TMA-modified zeolites contain a significant part of charge-compensating Al  
7 ions.  
8  
9

10  
11 The strong structural changes in the zeolites resulting from the reaction with TMA and  
12 subsequent treatment significantly affect their acidic properties. H/D exchange with C<sub>6</sub>D<sub>6</sub>  
13 measurements do not evidence an enhancement of the acidity of bridging hydroxyl groups with  
14 enhanced acidity in the modified zeolites. This is similar to the results reported previously for the  
15 EFAl-containing faujasites prepared by conventional incipient wetness impregnation and ion-  
16 exchange techniques.<sup>35</sup> Furthermore, these materials do not show a shift of the frequency of  
17 hydroxyl group to lower wavenumbers that is usually observed in the FTIR spectra of stabilized  
18 Y zeolites.<sup>61,62</sup> A fraction of the protons in AHFSY-TMA-Red shows acidity similar in strength  
19 to those in the parent AHFSY zeolite. The density of BAS in this material is only 10% of that in  
20 AHFSY. For the oxidized materials, this amounts to about 20% of the original BAS density. The  
21 BAS in the oxidized zeolites are somehow different from those in the reduced TMA-modified  
22 zeolite as their rate of H/D exchange is significantly lower. CO IR spectroscopy confirms the  
23 lower density of BAS in the TMA-modified zeolites. By using the shift of the OH groups upon  
24 CO perturbation as a criterion for acid strength, no significant differences in intrinsic proton  
25 acidities were observed. What stands out in the spectra of the reduced AHFSY-Red zeolite is the  
26 presence of strong Lewis acid sites as evidenced by the CO absorption band at 2222 cm<sup>-1</sup>. This  
27 band is attributed to the coordinatively unsaturated Al ions. We speculate that these ions perturb  
28 neighboring BAS. Upon oxidation, these strong Lewis acid sites completely disappear. The CO  
29  
30  
31  
32  
33  
34  
35  
36  
37  
38  
39  
40  
41  
42  
43  
44  
45  
46  
47  
48  
49  
50  
51  
52  
53  
54  
55  
56  
57  
58  
59  
60



IR spectra also show that all TMA-modified zeolites contain weak Lewis acid sites due to agglomerated forms of “Al-O” species.<sup>74</sup>

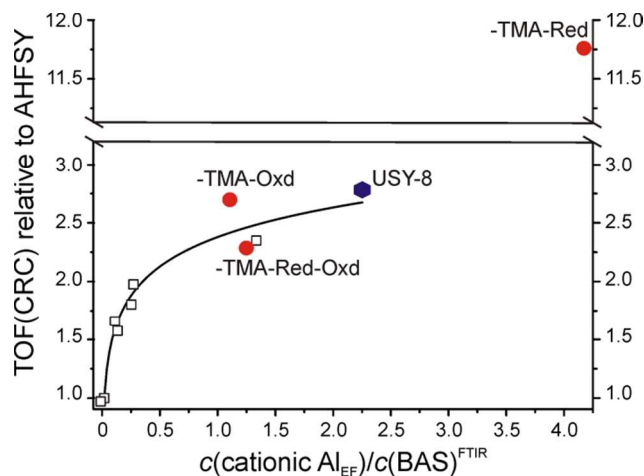


**Figure 7.** The propane cracking activity (TOF(CRC) normalized by the value for AHFSY) of different EFAl-containing faujasite catalysts as a function of the amount of cationic Al<sub>EF</sub> per BAS. The activities of TMA-modified AHFSY catalysts are shown with red circles. The concentration of cationic Al<sub>EF</sub> was calculated for these samples as  $c(\text{cationic Al}_{\text{EF}}) = c(\text{Al}_{\text{F}})_{\text{NMR}} - c(\text{BAS})^{\text{FTIR}}$ . The correlation line and the activities of reference USY-8 (blue hexagon) and of Al<sub>EF</sub>-AHFSY catalysts prepared by incipient wetness impregnation and ion exchange of aqueous solution of Al(NO<sub>3</sub>)<sub>3</sub> (open squares) are adopted from Ref. 35 without modification (in this case  $c(\text{cationic Al}_{\text{EF}}) = c(\text{Al}_{\text{F}})^{\text{XRD}} - c(\text{BAS})^{\text{FTIR}}$ ).

Despite these relatively small differences in the intrinsic Brønsted acidity, the TMA modification has a significant effect on the rate of propane conversion. From comparison of weight-based activities, one concludes that AHFSY-TMA-Red is more active than the parent AHFSY as well as a commercial USY cracking zeolite. Besides, when the activities are normalized per BAS, all of the TMA-modified zeolites exhibit a higher intrinsic propane conversion rate than the two reference zeolites. Importantly, the modification with TMA leads to a significant increase in the rate of propane dehydrogenation. The results support the previous proposal that Lewis acidic Al sites are involved in propane dehydrogenation.<sup>35</sup> From Table 7 and

1  
2  
3 the characterization results, it may be inferred then that the rate of propane dehydrogenation is  
4 the highest for the strong Lewis acidic groups in reduced AHFSY-TMA. Oxidation results in the  
5 formation of a weaker form of Lewis acidity and the Al dispersion will likely also be lower. In  
6  
7  
8  
9  
10  
11 any case, the oxidized Al species show a much lower rate of propane dehydrogenation.

12  
13 The most striking finding of the present study is the exceptionally high cracking activity of  
14 AHFSY-TMA-Red. Despite its low BAS density, the overall propane conversion rate was higher  
15 than that of the commercial USY zeolite. When normalized per BAS, the propane cracking  
16 activity is many times higher than that of the reference zeolites. In our previous study,<sup>35</sup> we  
17 proposed the existence of a correlation between the intrinsic cracking activity of EFAl-  
18 containing zeolites and the ratio of cationic extraframework aluminum species and BAS. Fig. 7  
19 shows this correlation including the data for the present study. Clearly, the oxidized TMA-  
20 modified zeolites follow the correlation. This is expected because the extraframework Al species  
21 are likely present in their oxidic form. When these species are not completely oxidized as in the  
22 reduced sample, they are much more active than expected based on this correlation. Acidity  
23 characterization showed that the BAS in AHFSY-TMA-Red are strongly polarized (<sup>1</sup>H NMR) by  
24 strong Lewis acid Al sites (CO IR). We propose that the unique enhancement of Brønsted acid  
25 catalytic activity of the reduced TMA-modified AHFSY zeolite is due to the presence of strongly  
26 polarizing Lewis acid sites resulting from the hydrogenolysis of grafted TMA in H<sub>2</sub>. Due to the  
27 strong heterogeneity and structural complexity of the zeolites after modification with TMA, it is  
28 not possible to firmly conclude on structural or mechanistic aspects of this acidity enhancement.  
29  
30  
31  
32  
33  
34  
35  
36  
37  
38  
39  
40  
41  
42  
43  
44  
45  
46  
47  
48  
49  
50  
51  
52  
53  
54  
55  
56  
57  
58  
59  
60  
However, the finding that CO IR and C<sub>6</sub>D<sub>6</sub> H/D exchange did not reveal any special properties of  
the BAS might suggest that the Lewis acid sites are involved in the protolytic cracking  
mechanism.

## 5. Conclusions

Chemical vapor deposition of trimethylaluminum (TMA) was explored as an approach for the introduction of extraframework aluminum in faujasite-type zeolites to prepare model EFAl-containing zeolite catalysts. The subsequent decomposition of the grafted organoaluminum species was investigated in hydrogen and oxygen atmosphere. Reaction of an extraframework Al free high-silica AHFSY zeolite with TMA leads to nearly complete substitution of the bridging hydroxyl groups with Al species. The reaction, however, does not produce uniform homogeneously distributed species. Whilst part of the BAS is replaced, the highly reactive TMA compound also reacts with the basic faujasite lattice leading to substantial framework distortions and even removal of Al from the framework. This is due to the opening of the Si-O-Al bridges and the formation of stable Si-CH<sub>3</sub> species. Decomposition of grafted TMA in H<sub>2</sub> leads to a very active zeolite catalyst for propane conversion. Its activity is significantly higher for propane cracking and dehydrogenation than that of the parent AHFSY zeolite and a commercial steam-calcined USY cracking zeolite. Although these effects are less pronounced when the precursor is oxidized, the propane conversion rates per proton are still higher than for the reference samples. Together with the extensive characterization, we infer that Lewis acidity can significantly alter the intrinsic activity of protons in zeolites. Firstly, strong Lewis acid sites are directly involved in propane dehydrogenation and, secondly, their proximity to BAS results in a pronounced enhancement of the rates of propane cracking. It cannot be excluded that these two effects are interrelated by a common mode of propane activation on Lewis acid sites. The effect is the strongest for the strong Lewis acid Al sites formed by the reductive treatment of the TMA-modified zeolite.

## Acknowledgment

Financial support was provided by SABIC.

## ASSOCIATED CONTENT

**Supporting Information.** Supplementary XRD, Ar physisorption, FTIR,  $^{29}\text{Si}$  MAS NMR,  $^1\text{H}$ - $\{^{27}\text{Al}\}$  TRAPDOR,  $^{27}\text{Al}$  MAS NMR results.

## AUTHOR INFORMATION

### Corresponding Author

\* [e.a.pidko@tue.nl](mailto:e.a.pidko@tue.nl) (Evgeny A. Pidko); [e.j.m.hensen@tue.nl](mailto:e.j.m.hensen@tue.nl) (Emiel J. M. Hensen)

### Author Contributions

The manuscript was written through contributions of all authors. All authors have given approval to the final version of the manuscript.

## REFERENCES

1. Corma, A. *Chem. Rev.* **1995**, *95*, 559.
2. Busca, G. *Chem. Rev.* **2007**, *107*, 5366.
3. Rabo, J. A.; Gajda, G. J. *Catal. Rev. Sci. Eng.* **1990**, *31*, 385.
4. van Santen, R. A.; Kramer, G. J. *Chem. Rev.* **1995**, *95*, 637.
5. Corma, A. *Curr. Opin, Solid State Mater. Sci.* **1997**, *2*, 63.
6. Pine, L. A.; Maher, P. J.; Wachter, W. K. *J. Catal.* **1984**, *85*, 466.
7. Sohn, J. R.; Decanio, S. J.; Fritz, P.O.; Lunsford, J. H. *J. Phys. Chem.* **1986**, *90*, 4847.
8. Fritz, P. O.; Lunsford, J. H. *J. Catal.* **1989**, *118*, 85.
9. Makarova, M. A.; Dwyer, J. J. *Phys. Chem.* **1993**, *97*, 6337.
10. Lago, R. M.; Haag, W. O.; Mikovsky, R. J.; Olson, D. H.; Hellring, S. D.; Schmitt, K. D.; Kerr, G. T. *Stud. Surf. Sci. Catal.* **1986**, *28*, 677.
11. Makarova, M. A.; Bates, S. P.; Dwyer, J. J. *Am. Chem. Soc.* **1995**, *117*, 11309.
12. Narbeshuber, T.F.; Brait, A.; Seshan, K.; Lercher, J.A. *Appl. Catal. A*, **1996**, *146*, 119.
13. Beyerlein, R. A.; McVicker, G. B.; Yacullo, L. N.; Ziemiak, J. J. *J. Phys. Chem.* **1988**, *92*, 1967.
14. Sohn, J. R.; DeCanio, S. J.; Lunsford, J. H.; O'Donnell, D. J. *Zeolites*. **1986**, *6*, 225.
15. DeCanio, S. J.; Sohn, J. R.; Fritz, P.O.; Lunsford, J.H. *J. Catal.* **1986**, *101*, 132.

- 1  
2  
3 16. Mota, C. J. A.; Bhering, D. L.; Rosenbach, N. *Angew. Chem. Int. Ed.* **2004**, *116*, 3112.  
4  
5  
6  
7 17. Gounder, R.; Jones, A. J.; Carr, R. T.; Iglesia, E. *J. Catal.* **2012**, *286*, 214.  
8  
9  
10 18. Agostini, G.; Lamberti, C.; Palin, L.; Milanesio, M.; Danilina, N.; Xu, B.; Janousch, M.;  
11  
12 van Bokhoven, J.A. *J. Am. Chem. Soc.* **2010**, *132*, 667.  
13  
14  
15 19. Huang, J.; Jiang, Y.; Marthala, V. R. R.; Thomas, B.; Romanova, E.; Hunger, M. J.  
16  
17 *Phys.Chem. C.* **2008**, *112*, 3811.  
18  
19 20. Jiao, J.; Altwasser, S. ; Wang, W.; Weitkamp, J. ; Hunger, M. *J. Phys. Chem. B.* **2004**, *108*,  
20  
21 14305.  
22  
23  
24 21. Jiao, J.; Kanellopoulos, Wang, W.; Ray, S. S.; Foerster, H.; Freude, D.; Hunger, M. *Phys.*  
25  
26 *Chem. Chem. Phys.* **2005**, *7*, 3221.  
27  
28  
29 22. Li, S. H.; Zheng, A. M.; Su, Y. C.; Zhang, H. L.; Chen, L.; Yang, J.; Ye, C. H.; Deng, F.  
30  
31 *J. Am. Chem. Soc.* **2007**, *129*, 11161.  
32  
33  
34 23. Li, S. H.; Huang, S. J.; Shen, W. L.; Zhang, H. L.; Fang, H. J.; Zheng, A. M.; Liu, S. B.;  
35  
36  
37 Deng, F. *J. Phys. Chem. C.* **2008**, *112*, 14486.  
38  
39  
40 24. Li, S. H.; Zheng, A. M.; Su, Y. C.; Fang, H. J.; Shen, W. L.; Yu, Z. W.; Chen, L.; Deng, F.  
41  
42  
43 *Phys. Chem. Chem. Phys.* **2010**, *12*, 3895.  
44  
45  
46 25. Yu, Z. W.; Zheng, A. M.; Wang, Q.; Chen, L.; Xu, J.; Amoureux, J. P.; Deng, F. *Angew.*  
47  
48 *Chem., Int. Ed.* **2010**, *49*, 8657  
49  
50  
51 26. Babitz, S.M.; Williams, B.A.; Miller, J.T.; Snurr, R.Q.; Haag, W.O. ; Kung, H.H. *Appl.*  
52  
53 *Catal. A* **1999**, *179*, 71.  
54  
55  
56  
57  
58  
59  
60

- 1  
2  
3 27. Kotrel, S.; Rosynek, M.P.; Lunsford, J.H. *J. Phys. Chem. B* **1999**, *103*, 818.  
4  
5  
6 28. van Bokhoven, J.A.; Williams, B.A.; Ji, W.; Koningsberger, D.C.; Kung, H.H.;  
7  
8 Narbeshuber, T.F.; Vinek, H.; Lercher, J.A. *J. Catal.* **1995**, *157*, 388.  
9  
10  
11 29. Haag, W.O. *Stud. Surf. Sci. Catal.* **1994**, *84*, 1375.  
12  
13  
14 30. Wei, J. *Chem. Eng. Sci.* **1996**, *51*, 2995.  
15  
16  
17  
18 31. Xu, B.; Sievers, C.; Hong, S.B.; Prins, R.; van Bokhoven, J.A. *J. Catal.* **2006**, *244*, 163.  
19  
20  
21 32. Ramachandran, C.E.; Williams, B.A.; van Bokhoven, J.A. Miller, J.T. *J. Catal.* **2005**, *233*,  
22  
23 100.  
24  
25  
26 33. Maesen, T.L.M. ; Beerdsen, E.; Calero, S.; Dubbeldam, D.; Smit B. *J. Catal.* **2006**, *237*,  
27  
28 278.  
29  
30  
31  
32 34. Xu, B.; Sievers, C.; Prins, R.; van Bokhoven, J.A. *Appl. Catal. A.* **2007**, *333*, 245.  
33  
34  
35 35. Almutairi, S. M. T.; Mezari, B.; Filonenko, G. A.; Magusin, P. C. M. M.; Rigutto, M. S.;  
36  
37 Pidko, E.A.; Hensen, E. J. M. *ChemCatChem*, **2013**, *5*, 452  
38  
39  
40 36. Copéret, C.; Chabanas, R.; Saint-Arroman, R. P.; Basset, J. M. *Angew. Chem. Int. Ed.* **2003**,  
41  
42 42, 156.  
43  
44  
45 37. García-Sánchez, Magusin, M.; P. C. M. M.; Hensen, E. J. M.; Thüne, P. C.; Rozanska, X.;  
46  
47 van Santen, R. A. *J. Catal.* **2003**, *219*, 352.  
48  
49  
50 38. Hensen, E. J. M.; Pidko, E. A.; Rane, N.; van Santen, R. A. *Angew. Chem. Int. Ed.* **2007**, *46*,  
51  
52 7273.  
53  
54  
55  
56  
57  
58  
59  
60

- 1  
2  
3  
4 39. Almutairi, S. M. T.; Mezari, B.; Magusin, P. C. M. M.; Pidko, E. A.; Hensen, E. J. M. *ACS*  
5  
6 *Catal.* **2012**, *2*, 71.  
7  
8  
9 40. Puurunen, R. L.; Lindblad, M.; Root, A.; Krause, A. O. I. *Phys. Chem. Chem. Phys.* **2001**, *3*,  
10  
11 1093.  
12  
13  
14 41. Van Looveren, L. K.; Geysen, D. F.; Vercruyssen, K. A.; Wouters, B. H.; Grobet, P. J.;  
15  
16 Jacobs, P. A. *Angew. Chem. Int. Ed.* **1998**, *37*, 517.  
17  
18  
19  
20 42. Bartram, M. E.; Michalske, T. A.; Rogers, J. W.; Mayer, T. M. *Chem. Mater.* **1991**, *3*, 953.  
21  
22  
23  
24 43. Boleslawski, M.; Serwatowski, J. J. *Organomet. Chem.* **1983**, *255*, 269.  
25  
26  
27 44. Pasykiewicz, S. *Polyhedron.* **1990**, *9*, 429.  
28  
29  
30 45. Siedle, A. R.; Newmark, R. A.; Lamanna, W. M.; Schroepfer, J. N. *Polyhedron.* **1990**, *9*,  
31  
32 301.  
33  
34  
35 46. Chien, J. C. W.; He, D. *J. Polym. Sci. Part A: Polym. Chem.* **1991**, *29*, 1603.  
36  
37  
38  
39 47. Korneev, N. N.; Khrapova, I. M.; Polonskii, A. V.; Ivanova, N. I.; Kisin, A. V.; Kolesov, V.  
40  
41 *S. Russ. Chem. Bull.* **1993**, 1453.  
42  
43  
44 48. Barron, A. R. *Macromol. Symp.* **1995**, *97*, 15.  
45  
46  
47 49. Harlan, C. J.; Bott, S. G.; Barron, A. R. *J. Am. Chem. Soc.* **1995**, *117*, 6465.  
48  
49  
50 50. Katayama, H.; Shiraishi, H.; Hino, T.; Ogane, T.; Imai, A. *Macromol. Symp.* **1995**, *97*, 109.  
51  
52  
53  
54 51. Lee, D. H.; Shin, S. Y. *Macromol. Symp.* **1995**, *97*, 195.  
55  
56  
57 52. Sinn, H. J. *Macromol. Symp.* **1995**, *97*, 27.  
58  
59  
60



- 1  
2  
3 53. Winter, H.; Schnuchel, W.; Sinn, H. *Macromol. Symp.* **1995**, *97*, 119.  
4  
5  
6 54. Reddy, S. S.; Radhakrishnan, K.; Sivaram, S. *Polym. Bull.* **1996**, *36*, 165.  
7  
8  
9  
10 55. Fusco, R.; Longo, L.; Masi, F.; Garbassi, F. *Macromol.* **1997**, *30*, 7673.  
11  
12  
13 56. *US patent* No. 20110137093 A1, **2011**.  
14  
15  
16 57. Sree, S. P.; Dendooven, J.; Korányi, T. I.; Vanbutsele, G.; Houthoofd, K.; Deduytsche, D.;  
17 Detavernier, C.; Martens, J. A. *Catal. Sci. Technol.* **2011**, *1*, 218.  
18  
19  
20  
21 58. Detavernier, C.; Dendooven, J.; Sree, S. P.; Ludwig, K. F.; Martens, J. A. *Chem. Soc. Rev.*  
22 **2011**, *40*, 5242.  
23  
24  
25  
26  
27 59. Cairon, O.; Chevreau, T.; Lavalley, J. C. *J. Chem. Soc. Faraday Trans.* **1998**, *94*, 3039.  
28  
29  
30  
31 60. Daniell, W.; Topsøe, N. Y.; Knözinger, H. *Langmuir* **2001**, *17*, 6233.  
32  
33  
34 61. Hensen, E. J. M.; Poduval, D. G.; Ligthart, D. A. J. M.; van Veen, J. A. R.; Rigutto, M. S. *J.*  
35 *Phys. Chem. C.* **2010**, *114*, 8363.  
36  
37  
38  
39 62. Poduval, D. G.; van Veen, J. A. R.; Rigutto, M. S.; Hensen, E. J. M. *Chem. Commun.* **2010**,  
40 *46*, 3466.  
41  
42  
43  
44  
45 63. Li, J.; DiVerdi, J. A.; Maciel G. E. *J. Am. Chem. Soc.* **2006**, *128*, 17093.  
46  
47  
48 64. Hensen, E. J. M.; Pidko, E. A.; Rane, N.; van Santen, R. A. *Stud. Surf. Sci. Catal.* **2007**, *170*,  
49 1182.  
50  
51  
52  
53 65. Van Eck, E.R.H.; Janssen, R.; Maas, W.E.J.R.; Veeman, W.S. *Chem. Phys. Lett.* **1990**, *174*,  
54 428.  
55  
56  
57  
58  
59  
60

- 1  
2  
3  
4  
5  
6  
7  
8  
9  
10  
11  
12  
13  
14  
15  
16  
17  
18  
19  
20  
21  
22  
23  
24  
25  
26  
27  
28  
29  
30  
31  
32  
33  
34  
35  
36  
37  
38  
39  
40  
41  
42  
43  
44  
45  
46  
47  
48  
49  
50  
51  
52  
53  
54  
55  
56  
57  
58  
59  
60
66. Grey, C.P.; Vega, A.J. *J. Am. Chem. Soc.* **1995**, *117*, 8232.
67. Engelhardt, G.; Michel, D. *High Resolution Solid State NMR of Silicates and Zeolites*, Wiley & Sons, New York, **1987**.
68. Massiot, D.; Fayon, F.; Capron, M.; King, I.; Le Calvé, S.; Alonso, B.; Durand, J.; Bujoli, B.; Gan, Z.; Hoatson, G. *Magn. Reson. Chem.* **2002**, *40*, 70.
69. Klinowski, J.; Ramdas, S.; Thomas, J.M.; Fyfe, C.A.; Hartman, J.S. *J. Chem. Soc., Faraday Trans. II* **1998**, *78*, 1025.
70. Kentgens, A. P. M.; Iuga, D.; Kalwei, M.; Koller, H. *J. Am. Chem. Soc.* **2001**, *123*, 2925.
71. Czjzek, G.; Fink, J.; Götz, F.; Schmidt, H.; Coey, J. M.; Rebouillat, J. P.; Liénard, A. *Phys. Rev. B* **1981**, *23*, 2513.
72. Kerber, R. N.; Kermagoret, A.; Callens, E.; Florian, P.; Massiot, D.; Lesage, A.; Copéret, C.; Delbecq, F.; Rozanska, X.; Sautet, P. *J. Am. Chem. Soc.* **2012**, *134*, 6767.
73. Fu, Q. J.; Ramirez-Cuesta, A. J.; Tsang, S. C. *J. Phys. Chem. B.* **2006**, *110*, 711.
74. Zecchina, A.; Platero, E. E.; Arean, C. O. *J. Catal.* **1987**, *107*, 244.

## Table of contents image

